

GMCP: A fully Global multi-source Merging-and-Calibration Precipitation dataset (1-hourly, 0.1°, global, 2000–Present)

Ziqiang Ma^{a,b*}; Jintao Xu^a; Bo Dong^c; Xie Hu^d; Hao Hu^{e,f}; Songkun Yan^a; Siyu Zhu^{a,g}; Kang He^h; Zhou Shiⁱ; Yun Chen^j; Xiang Fang^j; Qinghong Zhang^k; Songyan Gu^l; Fuzhong Weng^{e,f}

^a*Institute of Remote Sensing and Geographical Information Systems, School of Earth and Space Sciences,
Peking University, Beijing, 100871, China*

^b*International Research Centre of Big Data for Sustainable Development Goals, Beijing, China*

^c*National Centre for Earth Observation, Department of Meteorology, University of
Reading, Reading, United Kingdom*

^d*College of Urban and Environmental Sciences, Peking University, Beijing, 100871, China*

^e*CMA Earth System Modeling and Prediction Centre (CEMC), China Meteorological Administration,
Beijing 100081, China*

^f*State Key Laboratory of Severe Weather, Chinese Academy of Meteorological Sciences, China
Meteorological Administration, Beijing 100081, China*

^g*School of Civil Engineering and Environmental Science, University of Oklahoma, Norman, OK, United
States*

^h*Department of Civil and Environmental Engineering, University of Connecticut, Storrs, CT 06269, United
States*

ⁱ*Institute of Agricultural Remote Sensing and Information Technology Application, College of
Environmental and Resource Sciences, Zhejiang University, Hangzhou, 310058, China*

^j*National Meteorological Centre, China Meteorological Administration, Beijing, 100081, China*

^k*Department of Atmospheric and Oceanic Sciences, School of Physics, Peking University, Beijing, 100871,
China*

^l*National Satellite Meteorological Centre, China Meteorological Administration, Beijing, 100081, China*

Corresponding author: Dr. Ziqiang Ma (zqma@pku.edu.cn)

Early Online Release: This preliminary version has been accepted for publication in *Bulletin of the American Meteorological Society*, may be fully cited, and has been assigned DOI 10.1175/BAMS-D-24-0051.1. The final typeset copyedited article will replace the EOR at the above DOI when it is published.

© 2025 American Meteorological Society. This is an Author Accepted Manuscript distributed under the terms of the default AMS reuse license. For information regarding reuse and general copyright information, consult the AMS Copyright Policy (www.ametsoc.org/PUBSReuseLicenses).

ABSTRACT

Current global multi-source merged precipitation datasets can facilitate better utilization of the complementary nature of gauge-, satellite-, and reanalysis-based precipitation estimates, particularly for capturing precipitation variability. However, merging these datasets at high resolutions of 1-hourly and 0.1° on a full global scale remains a substantial challenge for the scientific community owing to high spatiotemporal heterogeneities. This study proposed a merging-and-calibration framework to optimally integrate the advantages of gauge-, satellite-, and model-based precipitation estimates, focusing on precipitation occurrences and providing a new fully Global multi-source Merging-and-Calibration Precipitation dataset (GMCP: 1-hourly, 0.1° , global, 2000–Present). The main conclusions included: (1) GMCP generally outperformed the input datasets, ERA5-Land, GSMAp-MVK, and IMERG-Late, across various spatiotemporal scales, both in regional statistics and extreme precipitation systems; (2) GMCP significantly outperformed IMERG-Final, calibrated by gauge analysis at the monthly scale, with the improvements in correlation coefficient (CC), root mean square error (RMSE), and Heidke skill score (HSS) by approximately 66.67%, 39.25%, and 26.83%, respectively, from 2016 to 2020 over the Continental United States (CONUS); (3) compared to the state-of-the-art multi-source merged product with a daily gauge correction scheme, MSWEP V2 (3-hourly and 0.1°), GMCP demonstrated the notable improvements with an approximately 20% enhancement in accurately capturing the precipitation occurrences against approximately 67,000 rain gauges over Mainland China in 2016; (4) in comparison to another well-known multi-source merged quasi-global daily and 0.05° precipitation product, CHIPRS integrating the gauge-, satellite-, and reanalysis-based precipitation estimates, GMCP also demonstrated the notable improvements at the daily scale, achieving the increases in CC, RMSE, and HSS by around 57.45%, 38.18%, and 75.76%, respectively, against approximately 67,000 rain gauges over Mainland China in 2016; and (5) this framework was suitable for generating the fully global precipitation datasets at 1-hourly and 0.1° scales, significantly mitigating the inherent shortcomings of each input dataset, with GMCP demonstrating the great potential as a valuable resource for worldwide scientific research and societal applications.

Keywords: Precipitation; Merging; Calibration; Multiplicative Triple Collocation; Global dataset

SIGNIFICANCE STATEMENT

Highly accurate global gridded precipitation datasets for precipitation occurrences and volumes are essential for understanding the water, energy, and carbon cycles on Earth in the context of a changing climate. This study aimed to introduce a new fully global multi-source merged precipitation dataset with high quality and resolutions of 1-hourly and 0.1° from 2000 to the present. This dataset integrated the advantages of ground gauge-, satellite-, and model-based precipitation estimates, particularly regarding precipitation occurrence, which can benefit scientific research communities and societal applications worldwide, including hydrological, climatological, meteorological, and water resource management.

CAPSULE

GMCP: A long-term fully global precipitation dataset (1-hourly, 0.1°, global, 2000–present) was developed by comprehensively considering both precipitation occurrences and volumes in multi-source merging and calibration processes.

1. Introduction

Precipitation is one of the most challenging meteorological variables owing to its high spatiotemporal heterogeneity (Hou et al., 2014; Huffman et al., 2019; Levizzani et al., 2020; Xu et al., 2023; Yan et al., 2023; Ji et al., 2024). Under climate warming scenarios, precipitation variability is expected to increase significantly, as indicated by the Clausius-Clapeyron relation, which suggests that the near-surface atmospheric moisture-holding capacity increases by approximately 7% per Kelvin, resulting in greater fluctuations in precipitation occurrences and wider swings between wet and dry episodes (Douville et al., 2021). For instance, recent investigations have revealed that accumulated anthropogenic warming has led to a global increase in daily precipitation variability of 1.2% per decade over 75% of land areas over the past century, posing new challenges for weather prediction and societal resilience (Zhang et al., 2024). Additionally, global warming is projected to cause robust increases in precipitation variability across various spatiotemporal scales, particularly at the synoptic scale (Zhang et al., 2021; Jiang et al., 2023). Therefore, it is essential to accurately monitor global precipitation occurrences and volumes at a high spatiotemporal resolution. Currently, there are three principal sources of precipitation information: ground gauge- and radar-based observations, satellite remote sensing, and atmospheric retrospective analysis models. However, precipitation data from these different sources possess their own advantages and disadvantages (Beck et al., 2017, 2019; Ma et al., 2020, 2022; for details of the mainstream datasets, see Table 1).

Ground rain gauges, weather radars, and ocean buoys provide accurate precipitation information at point or regional scales but lack global coverage. The accuracy of interpolation-based gauge analysis is highly dependent on the density of the gauge network and the degree of spatial coherence, both of which exhibit significant global variability (e.g., CPC-Gauge, 0.5°, daily, Xie et al., 2007; APHRODITE, 0.25°, daily, Yatagai et al., 2012, 2019; GPCC, 1.0°, daily, Adler et al., 2018). In contrast, satellites can observe large areas instantaneously at high resolutions, leading to the continuous launch of two international constellation-based satellite missions: the Tropical Rainfall Measuring Mission (TRMM) in 1997 and the Global Precipitation Measurement (GPM) mission in 2014 (Kummerow et al., 1998; Kidd and Levizzani, 2011; Hou et al., 2014). Satellite precipitation products can be categorized into two types: infrared (IR)-based precipitation estimates that utilize infrared observations from geostationary satellites at high resolutions of approximately 0.04° and half-hourly intervals

(e.g., PERSIANN-CCS, 0.04° , half-hourly, Hong et al., 2004; PERSIANN-CDR-CCS, 0.04° , 3-hourly, Sadeghi et al., 2021; FY4AQPE-MSA, 0.04° , ~15 min, Ma et al., 2022; PECA-FY4A, 0.04° , ~15 min, Zhu and Ma, 2022) and microwave (MW)-based precipitation products that adopt microwave observations (e.g., CMORPH, 0.04° , half-hourly, Joyce et al., 2004; GSMap-MVK, 0.1° , 1-hourly, Mega et al., 2019; IMERG-Late, 0.1° , half-hourly, Kummerow et al., 2015). Satellite-based precipitation estimates, particularly those using MW technology, capture precipitation patterns in the tropics, oceans, and low-altitude regions during wet seasons, such as summer, spring, and autumn. However, they are prone to systematic biases, are relatively insensitive to snowfall and light rainfall events, and tend to underperform over snow- and ice-covered surfaces, as well as in high-altitude and high-latitude regions, particularly during winter (Tang et al., 2020; Xu et al., 2022; Yan et al., 2023; Ji et al., 2024). For instance, IMERG performs significantly better in summer when temperatures are higher and precipitation is more abundant but struggles to detect the precipitation occurrences in winter. Although infrared (IR)-based precipitation estimates are primarily limited to exploring cloud top information and surface precipitation can generally perform worse than MW-based estimates, they (e.g., PCDR and CHIRPS) are more effective at detecting precipitation occurrences during winter owing to the advantages of infrared data in cold conditions (Tang et al., 2020; Ji et al., 2024). Additionally, MW-based estimates, including IMERG-Late Version 06, demonstrate reasonable performance on an hourly scale and effectively reproduce diurnal cycles, even in arid regions, by capturing peak times, magnitudes, and variations (Xu et al., 2022). Overall, there remains significant room for improvement in satellite-based estimates of snowfall during winter and in cold climates (Meng et al., 2017; Tang et al., 2020; Xu et al., 2022; Ji et al., 2024).

Atmospheric reanalysis models are crucial sources for generating full global precipitation estimates, including ERA5 (0.25° , hourly; Hersbach et al., 2020), ERA5-Land (0.1° , hourly; Muñoz-Sabater, 2019), MERRA-2 (0.5° , hourly; Gelaro et al. 2017), JRA-55 (0.5° , 3-hourly; Kobayashi et al. 2015), which are well-suited for simulating the evolution of large-scale weather systems. However, they poorly represent the variability associated with convection owing to their relatively low resolutions and deficiencies in the parameterizations of sub-grid processes (Muñoz-Sabater, 2019). Satellite precipitation estimates are relatively ineffective over snow- and ice-covered surfaces and struggle to detect snowfall under various conditions. Moreover, reanalysis models possess inherent advantages in estimating precipitation during cold seasons and in high-altitude and high-latitude regions, particularly for snowfall estimation,

which outperform rainfall estimation because most snow originates from non-convective large-scale synoptic weather systems (Hersbach et al., 2020; Muñoz-Sabater, 2019; Gelaro et al., 2017; Kobayashi et al., 2015; Tang et al., 2020). The reanalysis products can effectively capture precipitation during summer because they are better at estimating stratiform precipitation than convective precipitation, as demonstrated in northeastern China (Xu et al., 2022). However, reanalysis tends to consistently overestimate the precipitation frequency while underestimating the global intensity owing to deficiencies in the parameterization of the physical processes controlling precipitation generation (Trenberth and Zhang 2018; Ma et al., 2022). Furthermore, although reanalysis is acceptable on a daily scale, its performance degrades on an hourly scale owing to limitations in reproducing the peak time, magnitude, and variation of diurnal cycles, as observed with ERA5 (Tang et al., 2020; Xu et al., 2022).

Although ground gauges are available only regionally, they are widely considered to be the most reliable means of estimating precipitation and are often used to calibrate satellite-only or reanalysis-only precipitation estimates, mitigating systematic biases and random errors (Huffman et al., 2007; Ma et al., 2020, 2022). Multi-satellite-only precipitation estimates, such as IMERG-Late, (Huffman et al., 2019) are inherently affected by regional, seasonal, and diurnal systematic biases and random errors (Ebert et al., 2007). To calibrate the multi-satellite-only IMERG-Late, the GPCP SG (2.5° , monthly) was initially created by combining multi-satellite-only estimates, primarily based on MW and IR observations, with gauge analysis using an inverse-error-variance weighting strategy (Huffman et al., 1997; Adler et al., 2003, 2018). Subsequently, the volumes of the half-hourly IMERG-Late were calibrated by applying the ratios between the accumulated monthly IMERG-Late and GPCP SG at the corresponding spatiotemporal locations, resulting in the final calibrated estimates, IMERG-Final, which demonstrated superior performance at monthly and annual scales compared to the hourly and daily scales (Lu et al., 2020; Xu et al., 2019, 2022). Similarly, global atmospheric reanalysis data, such as ERA5 (0.25°) and ERA5-Land (0.1°), exhibit notable non-zero and often substantial random errors and biases (Hersbach et al., 2020; Xu et al., 2022; Ma et al., 2022). In response, Ma et al. (2020) developed a Daily Spatio-Temporal Disaggregation Algorithm (DSTDCA) to calibrate the IMERG-Final on a 0.25° daily scale using gauge analysis, APHRODITE (Yatagai et al., 2012), resulting in the generation of the Asian precipitation dataset AIMERG (0.1° , half-hourly, 2000–2015, Monsoon Asia). They demonstrated a significantly improved quality compared to IMERG-Final. Additionally, Ma et al. (2022)

proposed the Daily Total Volume Controlled Merging and Disaggregation Algorithm (DTVCMDA), an updated daily calibration method that anchored ERA5-Land under total volume control by APHRODITE at a 0.25° daily scale and developed a long-term precipitation dataset (AERA5-Asia: 1-hourly, 0.1° , 1951–2015, Monsoon Asia). This dataset significantly outperformed both ERA5-Land and IMERG-Final against ground observations in Mainland China. Although AIMERG and AERA5-Asia benefit from APHRODITE's Asian gauge analysis, which improves the hourly precipitation accuracy, their limited spatial coverage restricts their global applicability. Thus, there is a crucial need to develop fully global multi-source ensemble precipitation estimates as the “bench mark” with fine quality and resolution on a daily scale to calibrate hourly satellite-only or model-only precipitation estimates within a merging-and-calibration framework.

Multi-source precipitation dataset merging algorithms aim to integrate the strengths of various data sources, with gauge-based estimates contributing primarily to terrestrial surfaces, satellite data dominating at low- and mid-latitudes, and reanalysis data playing a key role at high latitudes (Beck et al., 2017, 2019). Over the past two decades, numerous merging algorithms have been developed, mainly using statistical and machine learning methods. Common statistical approaches include simple model averaging (SMA) (Shen et al., 2014), one outlier removed (OOA) (Shen et al., 2014), dynamic Bayesian model averaging (DBMA) (Ma et al., 2018; Yumnam et al., 2022), triple collocation (TC) (Lyv et al., 2020), multi-source weighted ensemble precipitation (MSWEP) (Beck et al., 2017, 2019), and morphology-based adaptive spatiotemporal merging algorithm (MASTMA) (Zhu et al., 2022). Compared with statistical methods, machine learning techniques offer greater potential for solving a wide range of problems, including classification, regression, and prediction (Lei et al., 2022). Various ML algorithms have been extensively applied in precipitation calibration and merging, including random forest (RF) (Baez-Villanueva et al., 2020), quantile regression forest (QRF) (Bhuiyan et al., 2018), gradient boosting decision tree (GBDT) (Lei et al., 2022) and extreme gradient boosting (XGBoost) (Lei et al., 2022), support vector machine (SVR) (Kumar et al., 2019), convolutional neural networks (CNN) (Le et al., 2020), deep neural networks (DNN) (Tao et al., 2016), artificial neural networks (ANN) (Wehbe et al., 2020), long short-term memory networks (LSTM) (Tang et al., 2021), and multiple deep learning-coupled models (Wu et al., 2020; Gavahi et al., 2023). For instance, Lei et al. (2022) explored the application of GBDT, XGBoost, and RF to merge six satellite- and reanalysis-based precipitation datasets for building

classification and regression models, incorporating environmental variables, such as DEM, longitude, latitude, wind speed, relative humidity, soil moisture, cloud cover, air temperature, and spatial autocorrelation, which significantly improved the estimation of precipitation occurrences and intensity. XGBoost presented high computational efficiency for large-scale datasets. Similarly, Gavahi et al. (2023) proposed a deep learning-based architecture combining 3D-CNN and ConvLSTM layers to capture spatial and temporal precipitation patterns using rain gauge observations as target values. The limitations of such algorithms are mainly: (1) their reliance on the density of gauge networks, which is particularly problematic in regions with cold climates, complex topography, snow, and glacier cover, where gauges are sparsely distributed and spatial heterogeneity is high; and (2) their applicability is largely confined to coarser spatiotemporal resolutions (e.g., monthly, daily, and 0.25°) and broader continental, national, or regional scales, failing to meet the demand for fully global precipitation datasets at high resolutions, such as hourly and 0.1° . Additionally, current regional, quasi-global, and fully global multi-source merged precipitation datasets focused mainly on the precipitation volumes, with insufficient attention given to precipitation occurrences (Beck et al., 2017, 2019; Ma et al., 2020, 2022), which presents challenges in capturing precipitation variability under a changing climate (Douville et al., 2021; Zhang et al., 2021; Jiang et al., 2023; Zhang et al., 2024).

Two scientific challenges should be addressed to generate a fully global, high-quality precipitation dataset at an hourly scale: (1) how to merge gauge-, satellite- and reanalysis-based precipitation datasets at daily and global scales, despite the severely uneven distribution of gauges, and (2) how to optimally estimate precipitation occurrences and volumes at an hourly scale without uniform global gauge data, as downscaling daily precipitation estimates to hourly data is difficult because of limited covariates and the complexity of their relationships (Ma et al., 2017, 2019, 2020). This study proposed a novel and flexible merging-and-calibration framework to address the concerns mentioned. First, it merged the gauge-, satellite-, and reanalysis-based precipitation datasets at daily and global scales, guided by point-based gauge information, and applied morphology and optimal theory (Zhu et al., 2022). Second, it combined satellite- and reanalysis-based estimates at an hourly scale using the updated triple collocation theory, focusing on precipitation occurrences without hourly gauge information guidance (Lyv et al., 2021; Ji et al., 2024). Finally, the hourly merged results

were calibrated using the daily merged data, as a global benchmark, following the calibration strategies of Ma et al. (2020, 2022).

The main objectives of this study were to (1) evaluating the reasonability and applicability of the proposed merging-and-calibration framework for multi-source precipitation merging at fully global 1-hourly and 0.1° scales, (2) provide a fully Global multi-source Merging-and-Calibration Precipitation dataset (GMCP: 1-hourly, 0.1° , 2000–Present) for scientific research and societal applications during the TRMM–GPM era, and (3) compare the performance of GMCP with contemporary state-of-the-art multi-source merged precipitation datasets at various spatiotemporal scales. Additionally, this study was conduct to offer references and possible merging-and-calibration schemes for future global ensemble precipitation products for operational purposes, based on various sources and algorithms at regional, quasi-global, and fully global scales.

Table 1. List of state-of-the-art satellite-based (S), gauge-based (G), and reanalysis (R) precipitation products. * denotes the datasets used in this study as input for driving the GMCP model.

Short name	Details	Data source(s)	Spatiotemporal resolution	Spatial coverage	Temporal coverage	References	Data sources
ERA-Interim	European Centre for Medium-Range Weather Forecasts (ECMWF) Reanalysis-Interim	R	80 km, 3 hourly	Global	1979 to 2019	Dee et al. (2011)	doi.org/10.5065/D6CR5RD9
ERA5*	European Centre for Medium-Range Weather Forecasts (ECMWF) Reanalysis-5	R	0.25°, hourly	Global	1979 to present	Hersbach et al. (2018,2020)	doi.org/10.24381/cds.adbb2d47
ERA5-Land*	European Centre for Medium-Range Weather Forecasts (ECMWF) Reanalysis-5-Land	R	0.1°, hourly	Global (land)	1981 to present	Muñoz-Sabater (2019a)	doi.org/10.24381/cds.e216bac
JRA-55	Japanese 55-year Reanalysis Modern-Era Retrospective Analysis for Research and Applications version 2	R	60 km, 3 hourly	Global	1955 to present	Kobayashi et al. (2015)	http://search.diasip.net/en/dataset/JRA55
MERRA-2	Integrated Multi-satellite Retrievals for Global Precipitation Measurement (IMERG)	R	0.5 °× 0.625°, hourly	Global	1980 to present	Gelaro et al. (2017)	https://disc.gsfc.nasa.gov/datasets?project=MERRA_2
IMERG*		S (Early, Late*); S+G (Final) S (MVK*); S+G (Gauge)	0.1°, halfhourly	Global	2000 to present	Huffman et al. (2019)	https://gpm.nasa.gov/data/directory/rainmap@hokusaicorc.jaxa.jp
GSMaP*	Global Satellite Mapping of Precipitation (GSMaP)	S	0.1°, hourly	Global	2000 to present	Ushio et al. (2009)	https://disc2.gesdisc.eosdis.nasa.gov/data/TRMM_L3/
TMPA	TRMM Multi-satellite Precipitation Analysis	S	0.25°, 3 hourly	50N to 50S	1998–2019	Huffman et al. (2007)	https://www.ncei.noaa.gov/data/cmorpho-high-resolution-global-precipitation-estimates/access/
CMORPH	CPC morphing technique (CMORPH)	S	0.07°, half hourly	60N to 60S	1998 to present	Joyce et al. (2004)	https://chrsdata.eng.uci.edu/
PERSIANN-CCS	Precipitation Estimation from Remotely Sensed Information using Artificial Neural Networks-Cloud Classification System	S	0.04°, half hourly	60N to 60S	2003 to present	Hong et al. (2004)	https://chrsdata.eng.uci.edu/
PERSIANN-CDR	Precipitation Estimation from Remotely Sensed Information using Artificial Neural Networks - Climate Data Record	S+G	0.25°, daily	60N to 60S	1983 to present	Ashouri et al. (2015)	https://chrsdata.eng.uci.edu/
GPCP	Global Precipitation Climatology Project monthly precipitation dataset Version 2.3	S+G	2.5°, monthly	Global	1979 to present	Adler et al. (2016)	doi.org/10.5067/MEASURES/GPCP/DATA304
CHIPS	Climate Hazards group Infrared Precipitation with Stations (CHIRPS) V2.0	S+G+R	0.05°, daily	50N to 50S (land)	1981 to present	Funk et al. (2015)	https://data.chc.ucsb.edu/products/CHIRPS-2.0/
MSWEP	Multi-Source Weighted-Ensemble Precipitation Asian Precipitation-Highly Resolved Observational Data Integration Towards Evaluation of Water Resources	S+G+R	0.1°, 3 hourly	Global	1979 to present	Beck et al. (2019)	https://www.glob20.org/mswep/
APHRODITE	Global Precipitation Climatology Centre (GPCC)	G	0.25°, daily	60E to 150E 55N to 15S (land)	1951 to 2015	Yatagai et al. (2012)	http://aphrodite.st.hirosaki-u.ac.jp/download/
GPCC	Full Data Daily Version 2018	G	1.0°, daily	Global (land)	1982 to 2016	Markus et al. (2018)	https://opendata.dwd.de/climate_environment/GPCC/html/download_gate.html

CPC-Gauge*	Climate Prediction Center (CPC) Unified Gauge-Based Analysis of Global Daily Precipitation	G	0.5°, daily	Global (land)	1979 to present	Xie et al. (2007) Chen et al. (2008)	https://ftp.cpc.ncep.noaa.gov/precip/CPC_UNI_PRCP/
GSOD*	Global Surface Summary of the Day	G	Stations, daily 4km, hourly	Global (land)	1929 to present	NCEI (1999)	ftp.ncdc.noaa.gov/pub/data/gsod
Stage-IV	Stage-IV gauge-adjusted, radar-based dataset	G		CONUS	2002 to present	Lin and Mitchell (2005)	https://data.col.ucar.edu/dataset/21.093

2. Data

Under the guidance that gauge-based precipitation estimates provide the primary contribution over terrestrial surfaces for all periods, with satellite data dominating at low- and mid-latitudes and reanalysis data at high latitudes (Beck et al., 2017, 2019), six precipitation datasets have been carefully utilized in the merging-calibration framework: GSOD, CPC-Gauge, GSMaP-MVK, IMERG-Late, ERA5, and ERA5-Land. CPC-Gauge is recognized as the most representative gauge analysis, offering the highest quality, resolution, and worldwide land coverage (Xie et al., 2007; Adler et al., 2018). For satellite-based estimates, IMERG-Late and GSMaP-MVK, were selected because of their performance compared to other contemporary satellite-based estimates, particularly IR-based estimates, such as PERSIANN-CCS, which utilizes IR information in their retrieval algorithms and data generation processes (Joyce et al., 2004; Kummerow et al., 2015; Mega et al., 2019; Tang et al., 2020; Xu et al., 2022). ERA5 over oceans and ERA5-Land over land were selected as the reanalysis estimates, as they demonstrated significant improvements over their predecessors, ERA-Interim, in both quality and resolution, and outperformed other reanalysis precipitation estimates, such as MERRA-2 and JRA-55 (Hersbach et al., 2020; Muñoz-Sabater., 2019; Gelaro et al., 2017; Kobayashi et al., 2015; Tang et al., 2020; Xu et al., 2022; Ji et al., 2024). Daily point-based GSOD data were applied to train the parameters for merging gauge-, satellite-, and reanalysis-based estimates on a daily scale (Menne et al., 2012; Zhu et al., 2022). Moreover, APHRODITE-Japan (Yatagai et al., 2012, 2019), CHIRPS (Funk et al., 2015), Stage IV, and ground point-based gauge precipitation data were selected for independent validation and comparison purposes. Detailed information regarding the selected precipitation datasets is as follows.

2.1 CPC-Gauge

The NOAA Climate Prediction Center (CPC) has developed a unified gauge-based analysis of global daily precipitation known as the CPC-Gauge (0.5° , 1979–present), which is the first product of the CPC Unified Precipitation Project (Xie et al., 2007; Chen et al., 2008). The primary objective of this project was to produce a suite of unified precipitation products with consistent quantities and enhanced quality by integrating all available information sources at CPC and utilizing the optimal interpolation (OI) objective analysis technique. CPC-Gauge data can be downloaded from the following website: https://ftp.cpc.ncep.noaa.gov/precip/CPC_UNI_PRCP/.

2.2 ERA5

ERA5 has significantly improved data quality, finer spatiotemporal resolution (1-hourly and 0.25°), and longer temporal spans (1950–present) than its widely used predecessor, ERA-Interim, owing to enhancements in model processes, core dynamics and data assimilation (Dee et al., 2011; Hersbach et al., 2020). It provides data on numerous atmospheric, land-surface and sea-state parameters, and its successful public release has facilitated further application across various scientific communities. In this study, the parameter of total precipitation in ERA5, which represents the total amount of liquid and frozen water (including rain and snow), was used. ERA5 can be available online at <https://doi.org/10.24381/cds.adbb2d47>.

2.3 ERA5-Land

The ERA5-Land dataset (0.1° , 1-hourly, 1950–present) is a replay of the land component of the ERA5 climate reanalysis, offering a consistent view of land parameter evolution over the past few decades at an enhanced resolution compared to ERA5 (Hersbach et al. 2020). The fine spatiotemporal resolution makes ERA5-Land particularly useful for various land surface applications and may serve as the first hourly dataset for describing water fluxes and energy balances on the global land surface at a spatial resolution of 0.1° for over 70 years (Ma et al., 2022). The total precipitation parameter from ERA5-Land was utilized in this study and is available at <https://doi.org/10.24381/cds.e2161bac>.

2.4 IMERG-Late

IMERG is a representative mapped precipitation product released by NASA that combines available microwave-based and infrared-based observations from the GPM constellation and geostationary satellites to provide comprehensive information on the microphysics and spatiotemporal variations of precipitation globally (Hou et al., 2014; Huffman et al., 2019, 2020). In this study, IMERG Late Run Version 06B (0.1° , half-hourly, ~ 18 h latency, hereafter referred to as IMERG-Late) was selected, utilizing both forward and backward morphing schemes. IMERG-Late can be accessed at <https://gpm.nasa.gov/data/directory>. Furthermore, the hourly scale precipitation dataset was derived by averaging the precipitation intensity from two corresponding half-hourly datasets within a specific hour.

2.5 GSMAp-MVK

GSMAp, developed by the Japan Aerospace Exploration Agency (JAXA), utilizes Dual-frequency Precipitation Radar (DPR) onboard the GPM core observatory, passive microwave

radiometers on GPM constellation satellites, and infrared sensors on geostationary satellites to provide an hourly global precipitation distribution map with a high spatial resolution of $0.1^\circ \times 0.1^\circ$ (Kubota et al., 2007). GSMP products include standard, near-real-time, real-time, and reanalysis products. In this study, we utilized the latest version 07 standard research product, GSMP-MVK, which does not incorporate gauge information corrections (Mega et al., 2019) and is available on the JAXA Global Watch website (<https://sharaku.eorc.jaxa.jp/GSMP>).

2.6 GSOD

The Global Surface Summary of the Day (GSOD) dataset includes precipitation information from approximately 12,000 certified global ground meteorological stations, and provides daily files summarizing the meteorological observations working in the corresponding days (NCEI, 1999). For each measurement day, the binary occurrences of fog, rain, snow, hail, thunder, tornado are recorded, in addition to common meteorological measurements, such as minimum and maximum temperatures, mean relative humidity, mean visibility, mean wind speed, and precipitation amount. GSOD data can be obtained from <https://www.ncei.noaa.gov/data/global-summary-of-the-day/archive/>.

2.7. APHRODITE

The Asian Precipitation – Highly Resolved Observational Data Integration Towards Evaluation (APHRODITE) dataset is a state-of-the-art gauge-based analysis dataset known for its finest spatiotemporal resolution and high quality data, integrating the largest number of ground observations from various Asian countries (Kamiguchi et al., 2010; Yatagai et al., 2012, 2019). Since its release, the APHRODITE dataset has garnered significant attention in water cycles-related investigations (Ji et al., 2020) and has been regarded as the “ground truth” or benchmark observations (Duncan and Bigg, 2012; Tan et al., 2020) for calibrating satellite-based precipitation retrievals, such as IMERG-Final (Ma et al., 2020). In this study, gridded daily precipitation of APHRODITE_Japan Version 1207 (0.05° , daily, 2009–2016; Kamiguchi et al., 2010) was adopted as the ground truth to evaluate the daily gridded precipitation estimates over Japan. The APHRODITE_Japan products can be accessed at <http://aphrodite.st.hirosaki-u.ac.jp/download/>.

2.8 CHIRPS

The Climate Hazards Group Infrared Precipitation with Stations dataset (CHIRPS, 0.05°, daily, 1981–present; Funk et al., 2015) was developed using ‘smart’ interpolation algorithms and high spatiotemporal resolution precipitation estimates derived from infrared Cold Cloud Duration observations. The key characteristics of CHIRPS include: (1) a 0.05° climatology that integrates satellite information to effectively represent sparsely gauged or non-gauged regions; (2) the provision of daily, pentadal, and monthly 0.05° Cold Cloud Duration-based precipitation estimates at the same resolution; (3) the incorporation of gauge network observational data to create a final product with an average latency of about approximately three weeks; and (4) the implementation of a novel blending strategy that utilizes the spatial correlation structure of Cold Cloud Duration estimates to assign interpolation weight. Furthermore, the CHIRPS is significant in various application fields, including hydrologic simulations, climate change assessments, and improved early warning. The CHIRPS products can be accessed at https://data.chc.ucsb.edu/products/CHIRPS-2.0/global_daily.

2.9 Stage IV

Stage IV analysis was derived from the multi-sensor hourly and 6-hourly “Stage III” analyses produced by the 12 River Forecast Centers (RFCs) in the contiguous United States (CONUS), which were based on local 4 km polar-stereographic grids. The National Centers for Environmental Prediction (NCEP) mosaics Stage III data into a national product, known as Stage IV, which offered 1-hourly, 6-hourly, and 24-hourly analyses (the latter accumulated from the 6-hourly data). Unlike NCEP Stage II, which lacked manual quality control (QC), Stage IV benefited from manual QC performed on Stage III data at the RFCs. As of April 2017, this dataset includes stations in Alaska and Puerto Rico. The Stage IV analysis utilized in this study can be accessed on the designated website <https://data.eol.ucar.edu/dataset/21.093>.

2.10 Ground point-based precipitation dataset

In this study, hourly rain gauge observations from approximately 67,000 Chinese meteorological stations were collected from the National Meteorological Information Center of the China Meteorological Administration for multiscale evaluation. These rain gauge precipitation datasets underwent three levels of quality control: extreme value, internal consistency, and spatial consistency checks (Shen et al., 2014). This ground point-based precipitation dataset has not been directly utilized in the merging-and-calibration framework proposed by this study. It is available at the hourly scale for Mainland China from the website <http://data.cma.cn>.

3. Methodology

3.1 Merging-and-Calibration framework for optimally integrating global multi-source precipitation datasets

Current algorithms have paid limited attention to generating global multi-source merged precipitation estimates that fully consider both precipitation occurrences and volumes simultaneously at high spatiotemporal resolutions of 1-hourly and 0.1° (Beck et al., 2017, 2019; Ma et al., 2020, 2022), posing challenges for revealing precipitation variability under changing climatic conditions (Douville et al., 2021; Zhang et al., 2021; Jiang et al., 2023; Zhang et al., 2024). To address this concern, this study proposed an advanced and practical merging-and-calibration framework for generating a fully global multi-source merged precipitation dataset with high resolution and quality for both precipitation occurrences and volumes. First, morphological and optimal theories were applied to consider these factors in the merging process of gauge-, satellite-, and reanalysis-based precipitation datasets on a daily scale guided by point-based gauge information (Zhu et al., 2022). Second, an updated triple collocation approach was proposed for merging satellite- and reanalysis-based estimates at an hourly scale, specifically addressing precipitation occurrences and volumes without hourly gauge information (Lyv et al., 2021; Ji et al., 2024). Finally, daily calibration strategies were adopted to calibrate the hourly merged results, using the daily merged results as the benchmark (Ma et al., 2020, 2022). This proposed framework consisted of six main steps: (1) spatiotemporally collocating multi-source precipitation datasets, (2) identifying global precipitation occurrence maps on a daily scale, (3) merging multi-source precipitation volumes on a daily scale, (4) identifying global precipitation occurrence maps on an hourly scale, (5) merging multi-source precipitation volumes on an hourly scale, and (6) calibrating hourly merged estimates using daily merged estimates under a total volume control strategy (Figure 1).

A. Spatiotemporally collocating the multi-source precipitation datasets

The basic global coverage and grid resolution were $-180^\circ - 180^\circ\text{N}$ and $-90^\circ - 90^\circ\text{E}$ at 0.1° , utilizing the World Geodetic System 1984 (WGS 84). Subsequently, CPC-Gauge (0.5°) and ERA5 (0.25°) were aligned to 0.1° using the nearest neighbor resampling strategy. Additionally, IMERG-Late (half-hourly, 0.1°), GSMP-MVK (1-hourly, 0.1°), and ERA5 and ERA5-Land (hourly, 0.1°) were accumulated on hourly and daily scales, respectively.

B. Identifying the global precipitation occurrence maps at daily scale

The morphology-based merging algorithm MASTMA can exhibit significant robustness in eliminating the negative effects of false alarm precipitation occurrences from multi-source precipitation products (Zhu et al., 2022). Consequently, MASTMA can be utilized to identify precipitation occurrences and merge the precipitation volumes on a daily scale. Based on morphological theory, the spatial morphological features (SMFs) for CPC-Gauge, ERA5, ERA5-Land, GSMP-MVK, and IMERG-Late were first generated on a global scale using an erosion strategy (see Figure 2 from Zhu et al., 2022). Next, point-based GSOD gauges were employed to extract SMFs from these products at 0.1° and daily scales. Finally, the reliability of the precipitation occurrences for each product were determined by quantifying the relationships between the SMFs and the precipitation occurrences recorded by the gauge-based GSOD at corresponding locations using sigmoid fitting functions. To account for the inadequacy of daily SMFs in constructing sigmoid fitting functions, the parameters for these functions were generated based on samples that combined daily SMFs with precipitation occurrence information from gauges in the corresponding month, resulting in monthly scale parameters for identifying precipitation occurrences. The precipitation probabilities derived from the sigmoid functions were then employed as weights alongside the precipitation occurrences from multi-source products to determine if a precipitation event occurred in the current grid. Ultimately, the merged precipitation occurrence map was established by weighted averaging of the precipitation occurrences from multi-source products, along with their corresponding weights from the sigmoid fitting functions, represented in binary records. In this study, a weighted average greater than 0.5 was set as the threshold for identifying precipitation occurrences.

C. Merging multi-source precipitation volumes at daily scale

Only pixels identified as precipitation occurrences occurring were considered when merging their precipitation volumes. Because of RMSEs of satellite- and model-based estimates, in comparison to ground observations, generally correlate with precipitation intensities (Huffman et al., 1997; Ma et al., 2020, 2022), this study employed RMSE as the weight for merging multi-source precipitation estimates. These weights were quantified using the average and standard deviation derived from the gauge-based GSOD and precipitation volumes from satellite and reanalysis products, as shown in Equation (1). The average and standard deviation were linearly fitted against the precipitation volumes, with specific intervals serving as the independent variables. Ultimately, the merged results were obtained by weighted

averaging of the multi-source precipitation volumes according to their corresponding weights derived from Equation (2). Detailed derivations of Equations (1) and (2) can be found in the study by Zhu et al. (2022).

$$RMSE = \sqrt{(avg - x)^2 + std^2} \quad (1)$$

$$w_k(x) = \frac{1}{RMSE_k} / (\sum_{k=1}^{Num} \frac{1}{RMSE_k}) \quad (2)$$

where x represents the precipitation volumes from satellite/reanalysis products; avg and std are the linearly fitted averages and standard deviations based on the samples with the gauge-based precipitation from GSOD and precipitation volumes from satellite/reanalysis products as the independent variable; w denotes the final merging weight for each product; and k represents the number of the multi-source products.

D. Identifying the precipitation occurrence maps for each product at hourly scale

Although there is limited hourly precipitation information from gauges on a global scale, distinguishing the weights of multi-source data from ground observations presents significant challenges. To mitigate false-alarm precipitation events from different sources while balancing computational efficiency and accuracy, a new erosion strategy was proposed to identify global precipitation occurrences on an hourly scale. Following careful comparisons of multi-source merged precipitation occurrences at a daily scale from step *B* with gauge-based records from GSOD, it was determined that the GSMAp-MVK exhibited relatively more accurate spatial patterns regarding precipitation occurrences. Thus it serves as a benchmark for trimming and distinguishing precipitation occurrences for IMERG-Late, ERA5 (over oceans), and ERA5-Land (over land). Additionally, two parameters, COV (coverage) and DIF (difference), were introduced to determine the erosion times for IMERG-Late, ERA5 (over oceans), and ERA5-Land (over land) on an hourly scale, referencing the spatial patterns of precipitation occurrences from GSMAp-MVK using Equations (3) – (5). These parameters were dynamically determined on the corresponding monthly scale by maximizing the target function TF, as outlined in Equation (5). Consequently, precipitation occurrence maps for each product, along with their corresponding precipitation volumes, were established on an hourly scale.

$$COV = (S_reference \cap S_others) / S_reference \quad (3)$$

$$DIF = (S_others - S_reference \cap S_others) / S_global \quad (4)$$

$$TF = COV - 2DIF \quad (5)$$

where *reference* represent GSMP-MVK; *others* stands for IMERG-Late, ERA5 (over oceans) and ERA5-Land (over land); S represents the area of precipitation occurrence map from GSMP-MVK; S_{global} denotes the entire area over globe; and TF is the target function.

E. Merging multi-source precipitation volumes at hourly scale

Once the precipitation occurrence maps for each product and their corresponding hourly precipitation volumes are determined, merging these volumes becomes a critical issue, particularly when there is limited or no global uniform gauge information or references on an hourly scale. To address this, we applied the multiplicative triple collocation (MTC) theory (Lyu et al., 2021), a reasonable method originally designed to quantify the uncertainties of three datasets with mutually independent errors without requiring a reference truth (Stoffelen, 1998). TC is extended by Alemohammad et al. (2015), suitable for multiplicative TC (MTC). Additionally, Lyu et al. (2020) compared the performances of two weighting strategies using MTC: logarithmic RMSE (log-RMSE) and modified RMSE (mod-RMSE), concluding that log-RMSE outperformed mod-RMSE due to the potential issues with underestimated inputs when using mod-RMSE. Consequently, this study utilized MTC with log-RMSE as its weighting strategy (Lyu et al., 2021) to merge the eroded hourly precipitation estimates from IMERG-Late, ERA5 (over oceans), ERA5-Land (over land), and GSMP-MVK in mid- and low-latitude regions (60°N – 60°S), thereby generating hourly merged precipitation estimates while considering precipitation occurrences. Furthermore, owing to the suboptimal performance of satellite-based precipitation products in cold areas, ERA5-Merged that combined ERA5 over oceans and ERA5-Land over land was regarded as a unique reference for high-latitude regions (60°N – 90°N and 60°S – 90°S) (Tang et al., 2021; Xu et al., 2022; Yan et al., 2023; Ji et al., 2024).

F. Calibrating the hourly merged estimates using the daily merged estimates under the total volume control strategy

At this stage, the global daily merged precipitation estimates (daily, 0.1°) from Step C were utilized as the ‘ground truth’ to calibrate and trim the global hourly merged results (hourly, 0.1°) from Step E, employing a total volume control strategy that referenced spatiotemporal disaggregation and calibration algorithms (DSTDCA, Ma et al., 2020; DTVCMDA, Ma et al., 2022). Specifically, the ratios of the merged hourly estimate to the accumulated daily result for the corresponding day served as weights to disaggregate the global daily merged results for the

respective pixels. A situation requiring further processing could occur when the daily merged result detected precipitation occurrences, whereas the hourly accumulated result did not. In such cases, the hourly merged zero values were updated by equally disaggregating the daily merged results across 24 periods in the corresponding grid. After completing these procedures, the final GMCP dataset (1-hourly, 0.1° , 2000–present, global) was generated, with the main structure shown in Figure 1. One thing needs to be noted is that the GMCP would be updated on a monthly scale to guarantee the parameters could be thoroughly trained, in step *B*, by all the point-based GSOD gauges for the fully global scale.

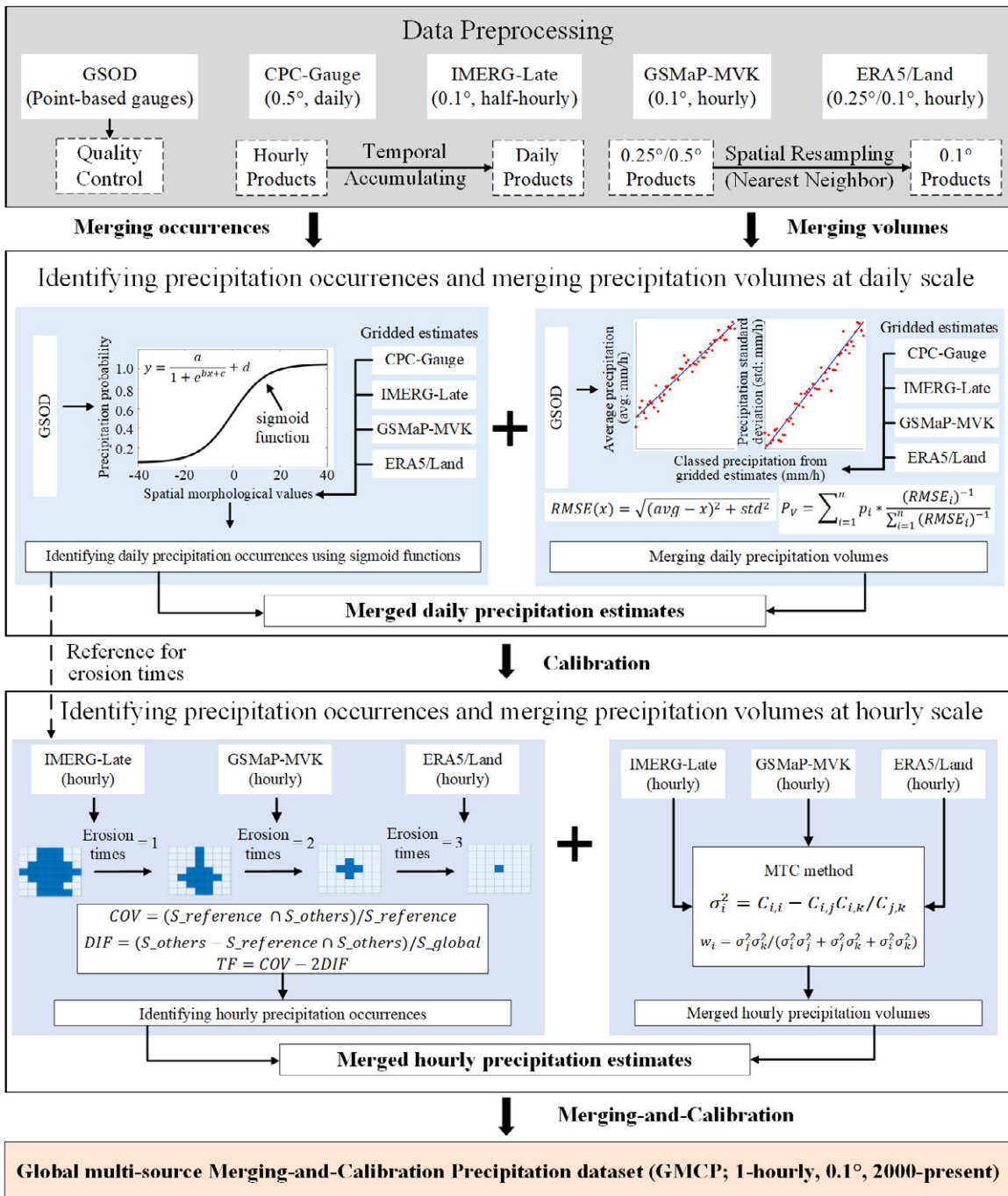


Figure 1. Flowchart of Dynamical Merging-and-Calibration framework for generating GMCP dataset.

3.2 Evaluation metrics

To comprehensively evaluate the performance of GMCP, ERA5-Land, GSMAp-MVK, IMERG-Late, IMERG-Final, MSWEP V2, and CHIPRS against point-based ground precipitation observations, gridded Stage IV, and APHRODITE_Japan, this study employed three classical continuous verification metrics, including CC, Bias, and root mean square error (RMSE), along with a comprehensive diagnostic verification metric, HSS. CC reflects the strength of the relationships between the estimated and observed datasets, where Bias and

RMSE indicate the degree of deviation between these datasets. HSS represents the capability of precipitation estimates to accurately capture precipitation occurrences and has been commonly used as a diagnostic verification metric (Ebert et al., 2007; Ma et al., 2022). This summary metric considers both the probability of detection and false-alarm ratios. The rain/no-rain thresholds were set at 0.1 mm for hourly scale evaluations and 1.0 mm for daily scale evaluations (Tang et al., 2020). The equations, value ranges, and perfect values of the verification metrics are listed in Table 2. The spatial and numerical distributions of these metrics were calculated at different temporal scales at corresponding points or grids, incorporating ground-based gauge or radar information over periods spanning one to several years and covering various climatological regions and seasons. For instance, hourly and daily metric values were computed using pairs of precipitation information from gauges and satellite- or reanalysis-based gridded precipitation products at specific rain gauges throughout the study period. Additionally, the temporal patterns of metrics were derived from pairs across all rain gauges in designated areas over various temporal scales, including hourly and daily.

Table2. List of the continuous and diagnostic verification metrics for evaluating precipitation products in this study.

Metrics names	Equations	Value Ranges (Perfect Values)
correlation coefficient (CC)	$CC = \sqrt{\frac{\sum_{i=1}^n (O_i - \bar{O})(E_i - \bar{E})}{\sum_{i=1}^n (O_i - \bar{O})^2 \times \sum_{i=1}^n (E_i - \bar{E})^2}}$	[-1, 1] (1)
relative bias (Bias)	$\text{bias} = \frac{\sum_{i=1}^n (E_i - O_i)}{\sum_{i=1}^n O_i}$	[-∞, +∞] (0)
root mean square error (RMSE)	$\text{RMSE} = \sqrt{\frac{1}{n} \sum_{i=1}^n (E_i - O_i)^2}$	[0, +∞] (0)
heidke skill score (HSS)	$\text{HSS} = \frac{2(HZ - FM)}{(H + M)(Z + M) + (H + F)(Z + F)}$	(-∞, 1] (1)

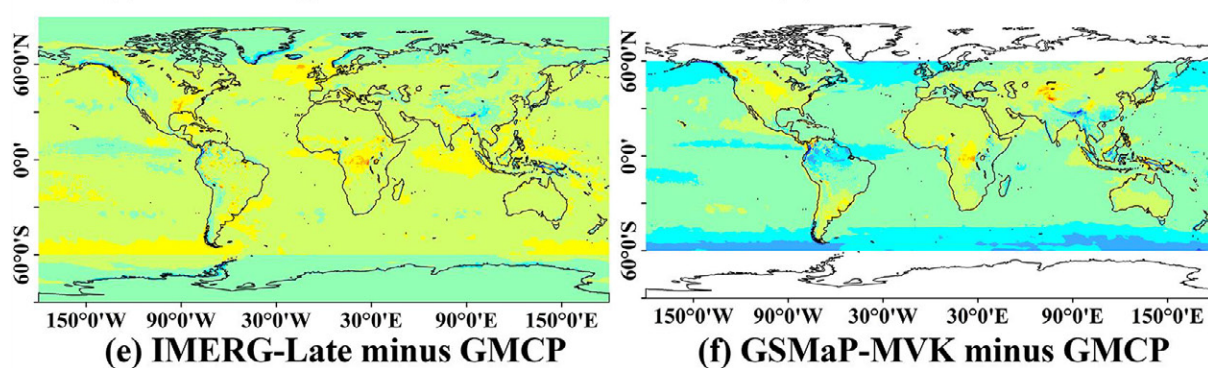
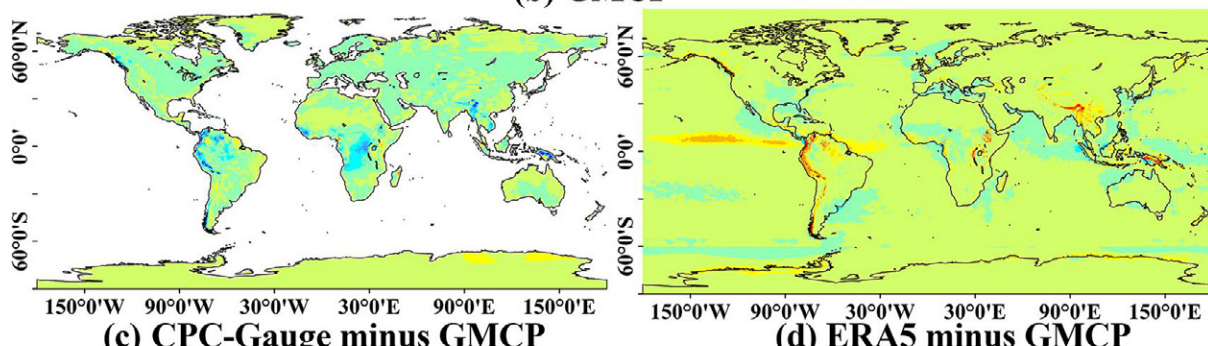
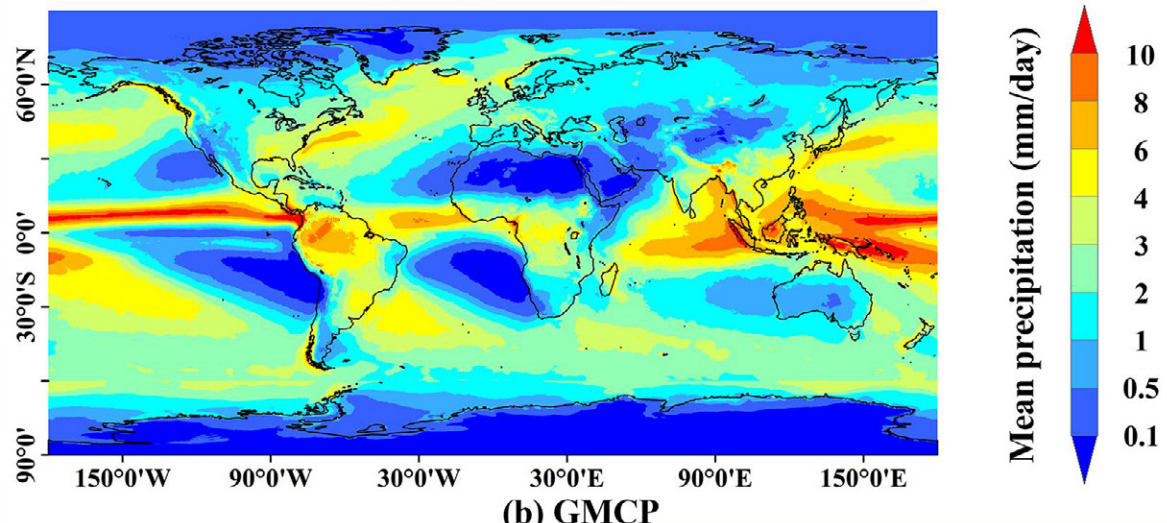
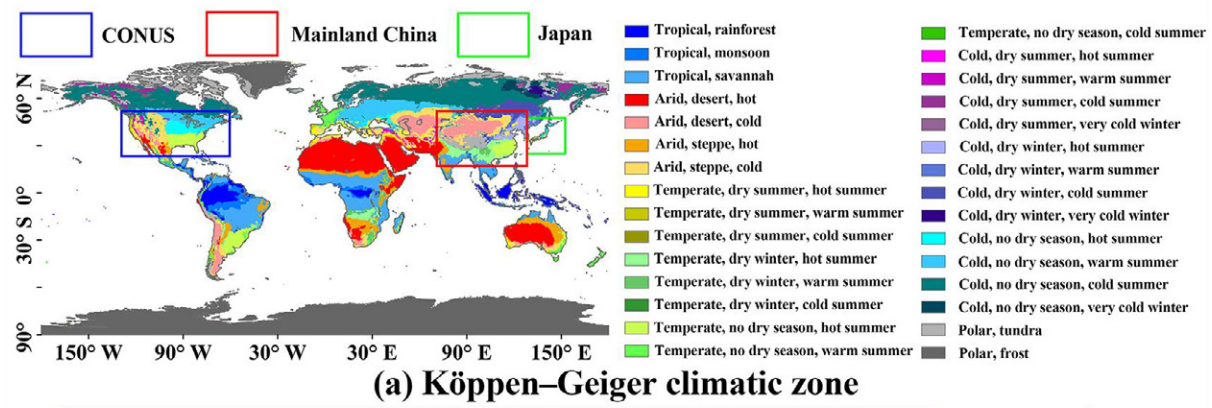
Note: O_i , observed precipitation; \bar{O} , mean observed precipitation; E_i , estimated precipitation; \bar{E} , average estimated precipitation; n, the number of precipitation pairs in the analysis; H, hit cases, when both observations and estimates are greater than the rain/no-rain threshold; M, missed occurrences, when observations are greater than or equal to the rain/no-rain threshold, but estimates are less than the rain/no-rain threshold; F, false alarms, when estimates are greater than or equal to the rain/no-rain threshold, but observations are less than the rain/no-rain threshold; Z, correct no-rain detection, when both observations and estimates are less than the rain/no-rain threshold.

4. Results

4.1 GMCP product

Figure 2 illustrates the global spatial distributions of the Köppen–Geiger climatic zones, the mean daily precipitation volumes of GMCP (0.1°), and the differences in mean daily precipitation volumes between CPC-Gauge, ERA5, IMERG-Late, GSMap-MVK and GMCP, respectively, for the period from January 1 2001, to December 31, 2020. Overall, GMCP effectively captured the general spatial patterns of global precipitation (Figure 2b), with significant precipitation volumes observed in tropical regions and minimal volumes in the

Antarctic, Arctic, and desert areas, such as the Sahara, Arabian Desert, and Lut Desert. Among the datasets, CPC-Gauge exhibited the closest similarity to GMCP, with absolute annual differences of less than approximately 1.0 mm/day globally, whereas relatively larger discrepancies were observed in the southern polar frost regions of northwestern South America, central Africa, Himalayas to the Hengduan Mountains, and New Guinea (Figure 2c). Conversely, ERA5 tended to overestimate the precipitation volumes compared to GMCP, particularly in the eastern central Pacific Ocean, along the western coastlines of South America, in the Himalayan to Hengduan Mountain region, and in New Guinea (Figure 2d). IMERG-Late generally overestimated the precipitation volumes in lower latitude regions between 60°S and 60°N, while underestimating the precipitation volumes in higher latitude regions from 60°S to 90°S and 60°N to 90°N, with GMCP serving as the reference. Notably, IMERG-Late exhibited a distinct spatial discontinuity in the transition from south to north along a latitude of approximately 60°N globally, primarily because of differing production strategies for regions on either side of this latitude, a concern that has been addressed in the GMCP dataset (Figure 2e). In contrast, GSMP-MVK tended to overestimate the precipitation volumes over land regions, except for northwestern South Africa, the southern Himalayas, and the Indonesian Peninsula, while underestimating the precipitation volumes over oceans, particularly in the southern oceans along the belt from 60°S to 50°S (Figure 2f). Moreover, CONUS, Mainland China, and Japan were selected as the regions of interest for further comparisons of the performance of GMCP and contemporary state-of-the-art gridded precipitation datasets in subsequent sections, as illustrated in Figure 2a, considering the density of ground observations and the complex topography and climatological zones.



Differences of precipitation volumes (mm/day)

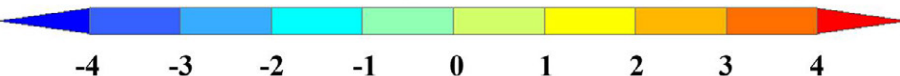


Figure 2. Global spatial distributions of (a) Köppen–Geiger climatic zones, (b) the mean daily precipitation volumes of GMCP (0.1°), and the differences in mean daily precipitation volumes between (c) CPC-Gauge and GMCP, (d) ERA5 and GMCP, (e) IMERG-Late, and (f) GSMAp-MVK and GMCP in the period 2001–2020.

The global spatial distributions of the mean annual number of precipitation occurrences for GMCP (0.1°) and the differences in mean annual precipitation occurrences between ERA5, IMERG-Late, GSMAp-MVK, and GMCP, respectively, from 2001 to 2020 are illustrated in Figure 3. According to GMCP, significant precipitation occurrences were primarily concentrated in the tropics, southeastern Asia, the northern Pacific and Atlantic Oceans, and the southern oceans along the belt of 60°S to 30°S , whereas minimal precipitation occurrences were observed in the Antarctic, Arctic, and regions spanning from the Sahara and Arabian Deserts to Lut Desert and Tibetan Plateau, as well as in certain ocean areas near the Atacama Desert and southern South Africa (Figure 3a). Using GMCP as a reference, ERA5 was found to generally overestimate precipitation occurrences, especially over the tropical Atlantic and eastern Pacific Oceans, the Sahara Desert, and the southern oceans along the belt from 60°S to 30°S (Figure 3b). Similarly, IMERG-Late tended to overestimate the precipitation occurrences globally, particularly in tropical regions such as the Sahara Desert, while underestimating precipitation occurrences in certain areas along the tropical oceans (Figure 3c). GSMAp-MVK displayed spatial patterns in estimating precipitation occurrences that were similar to those of IMERG-Late in the regions between 60°S and 60°N , albeit with relatively lower magnitudes, and demonstrated an underestimation of the precipitation occurrences over the southern oceans along the belt from 60°S to 30°S (Figure 3d).

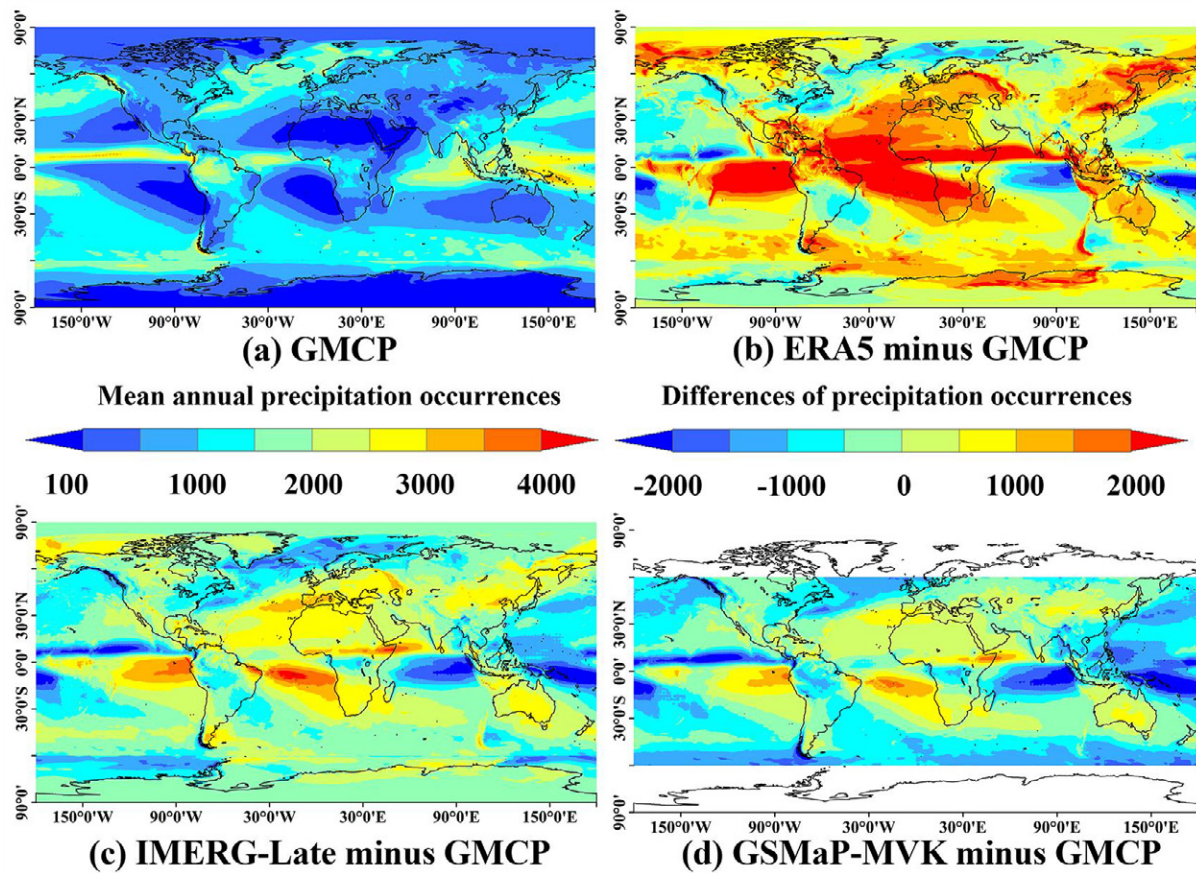


Figure 3. Global spatial distributions of (a) the mean annual number of precipitation occurrences of GMCP (0.1°) and the differences in mean annual precipitation occurrences between (b) ERA5, (c) IMERG-Late, (d) GSMAp-MVK, and GMCP, respectively, from 2001 to 2020.

4.2 Overall performances of GMCP

GMCP was compared with model- and satellite-based precipitation datasets at the hourly scale against the Stage IV gauge-radar dataset as the ground truth over CONUS. The spatial distributions of the evaluation results based on two classical continuous verification metrics (CC and RMSE) and one comprehensive diagnostic verification metric, HSS, for the period from January 1, 2016, to December 31, 2020, are presented in Figure 4. Overall, GMCP outperformed the other datasets in CONUS in terms of CC, RMSE, and HSS by effectively integrating the advantages of the input datasets. Specifically, for CC, GMCP capitalized on the strengths of ERA5-Land in western and northeastern CONUS and those of GSMAp-MVK and IMERG-Late in southeastern CONUS. In terms of RMSE, GMCP consistently exhibited superior performance and demonstrated similar distributions to ERA5-Land, whereas GSMAp-MVK performed the least favorably, particularly across central CONUS, with RMSE values exceeding 1.8 mm/hour, followed by IMERG-Late. In terms of HSS, GMCP significantly surpassed ERA5-Land, GSMAp-MVK, and IMERG-Late in most regions, with HSS values

greater than 0.5. Generally, the model-based precipitation estimates, particularly ERA5-Land, performed better than two satellite-based estimates, GSMAp-MVK and IMERG-Late, across the three evaluated metrics, likely because of the assimilation of ground radar observations in atmospheric analysis models (Hersbach et al., 2020; Muñoz-Sabater, 2019). Despite these advantages, GMCP still outperformed ERA5-Land, especially in CC and HSS, highlighting that GMCP effectively inherited the benefits of both satellite-based and ground-based estimates.

Although IMERG-Final is a calibrated product based on IMERG-Late, the improvements in CC and HSS are not significant, indicating limited calibration capabilities owing to the coarse resolutions of the calibration coefficients derived from the GPCP dataset at monthly and 1.0° scales. However, IMERG-Final exhibited significant improvements in RMSE, suggesting that the calibration algorithm effectively adjusted the precipitation volumes. In comparison, the calibrated satellite-based precipitation product GMCP (CC \sim 0.45, RMSE \sim 0.65 mm/hour, and HSS \sim 0.52) outperformed IMERG-Final (CC \sim 0.27, RMSE \sim 1.07 mm/hour, and HSS \sim 0.41), with the enhancements in CC, RMSE, and HSS of approximately 66.67%, 39.25%, and 26.83%, respectively, for the period from January 1, 2016, to December 31, 2020. This demonstrated that the merging-and-calibration framework had significant potential for integrating the advantages of multi-source precipitation products at finer resolutions.

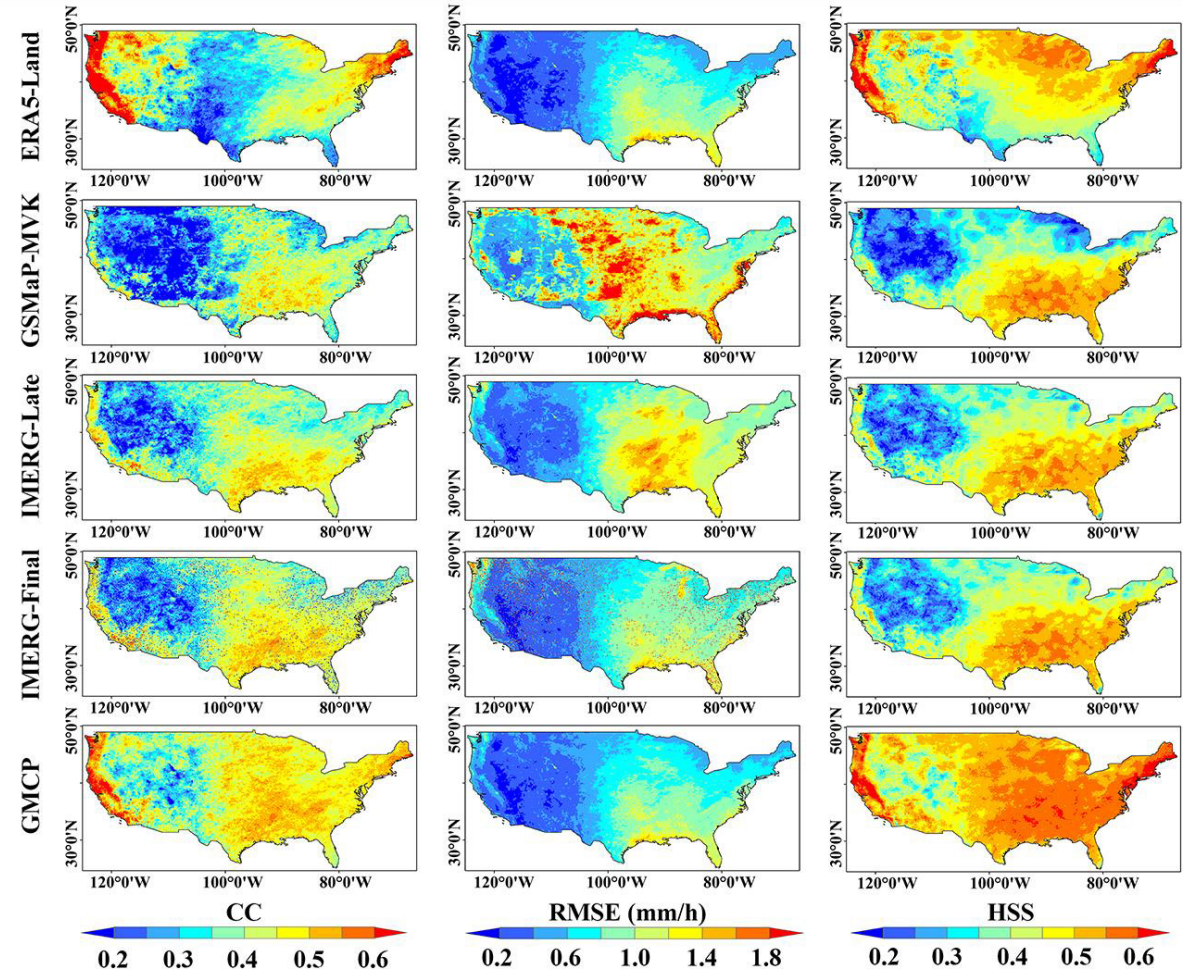


Figure 4. Spatial distributions of the three verification metrics (CC, RMSE, and HSS) over CONUS of hourly precipitation datasets, ERA5-Land, GSMAp-MVK, IMERG-Late, IMERG-Final, and GMCP against the Stage IV gauge-radar dataset as the reference, in the period from January 1, 2016 to December 31, 2020.

The GMCP dataset was further compared with ERA5-Land, GSMAp-MVK, IMERG-Late, and IMERG-Final on an hourly scale to accurately capture precipitation volumes and occurrences across Mainland China. The spatial distributions of CC, RMSE, and HSS, against approximately 67,000 rain gauge observations from January 1, to December 31, 2016, are shown in Figure 5. GMCP outperformed the other products, with larger CC and HSS values and smaller RMSE values. Specifically, the GMCP's performance is comparable to IMERG-Final and IMERG-Late, with CC values exceeding 0.35 at the majority of gauges, significantly surpassing GSMAp-MVK and ERA5-Land. In terms of RMSE, ERA5-Land performed well, closely approaching GMCP, whereas GSMAp-MVK exhibited the poorest performance across extensive regions, with RMSE values exceeding 1.8 mm/h. In terms of HSS, although ERA5-Land, GSMAp-MVK, and IMERG-Late demonstrated reasonable performance, GMCP distinctly outperformed them, achieving HSS values greater than 0.50

for the majority of gauges. Overall, GMCP surpassed ERA5-Land, GSMP-MVK, IMERG-Late, and IMERG-Final across all three metrics in Mainland China. Furthermore, GMCP notably outperformed the calibrated satellite-based precipitation dataset, IMERG-Final, particularly in HSS, with an improvement of approximately 17.95% from January 1, to December 31, 2016.

The analysis of the performance of these products in Mainland China and CONUS revealed three significant findings. First, the model-based ERA5-Land did not significantly outperform the satellite-based IMERG-Late and actually performed worse in terms of CC and HSS, which may be attributed to the limited ground observations assimilated into the ERA models over Mainland China (Hersbach et al., 2020; Muñoz-Sabater, 2019). Second, the improvements in IMERG-Final were modest, indicating its limited calibration capabilities due to the coarse resolution of calibration coefficients from the GPCP dataset at monthly and 1.0° resolutions. Third, GMCP demonstrated great potential by effectively inheriting the advantages of model-based, satellite-based, and ground-based estimates, while also alleviating the negative effects from each input precipitation dataset that drives the merging model for generating the GMCP.

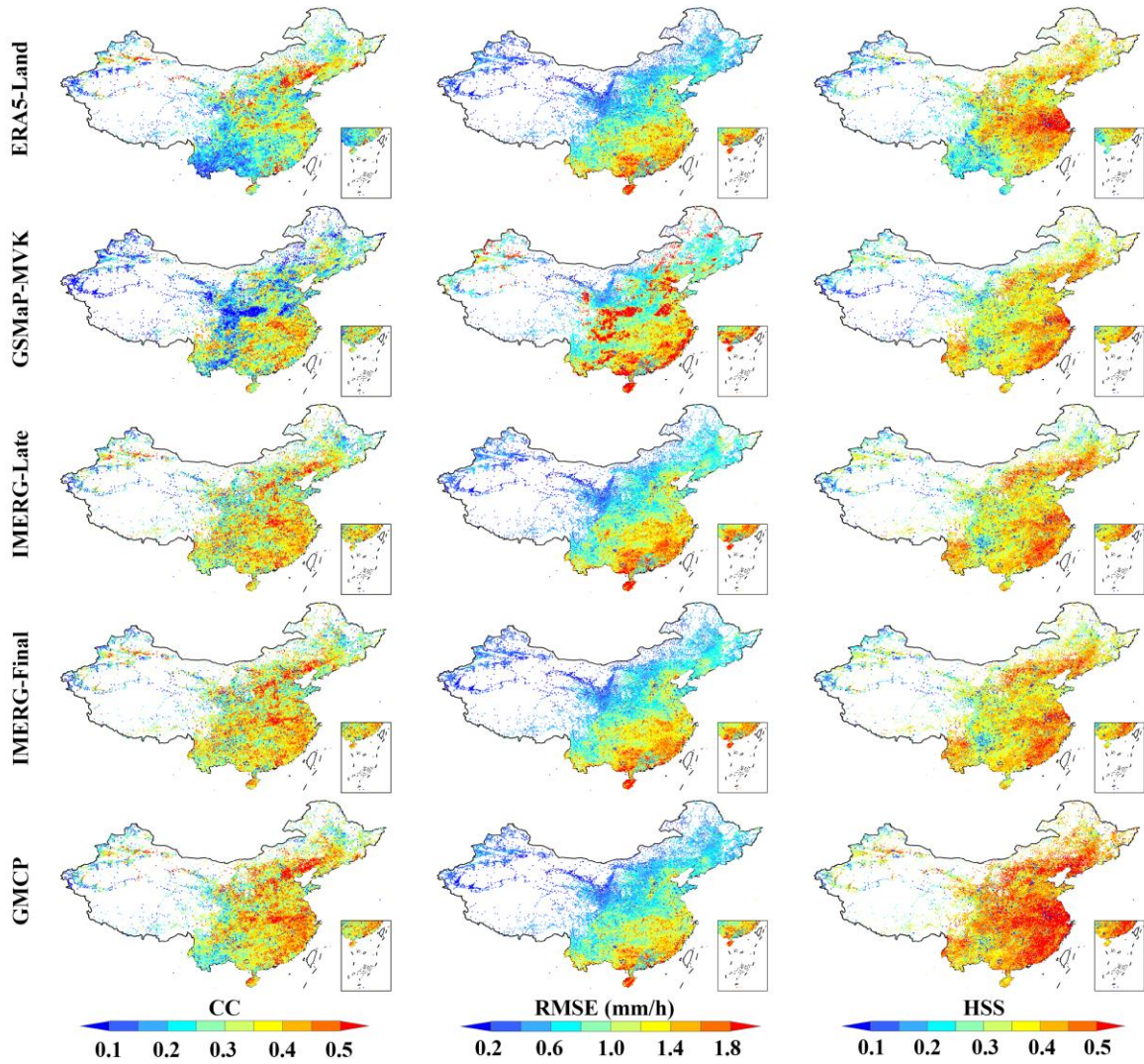


Figure 5. Spatial distributions of three verification metrics (CC, RMSE, and HSS) over Mainland China of hourly precipitation datasets, ERA5-Land, GSMAp-MVK, IMERG-Late, IMERG-Final, and GMCP against $\sim 67,000$ rain gauges as the reference, in the period from January 1, to December 31, 2016.

As GMCP dataset provides hourly precipitation estimates, it is really necessary to investigate whether GMCP has the ability to capture the characteristics of the diurnal precipitation variations. The average diurnal cycles of ERA5-Land, GSMAp-MVK, IMERG-Late, IMERG-Final, GMCP and Gauges, at the corresponding $\sim 67,000$ rain gauges, in the period from January 1, to December 31, 2016, over Mainland China are shown in Figure 6. It could be clearly seen that GMCP demonstrated the most closely diurnal variations with those of gauges both in magnitudes and phases, followed by IMERG-Late and IMERG-Final. Though ERA-Land has quietly larger magnitudes, it is still useful for capturing the two peaks over Mainland China with the smaller one occurring at 21:00 UTC and the larger one occurring at 8:00 UTC. However, GSMAp-MVK has four peaks happening at 3:00, 10:00, 14:00, and

20:00 UTC, respectively, demonstrating the least abilities to capture the diurnal variations over Mainland China. Therefore, the capability of GMCP in revealing the diurnal precipitation variations furtherly illustrates the robustness of the merging-and-calibration framework proposed by this study for optimally combining the ERA5, GSMAp-MVK, and IMERG-Late together.

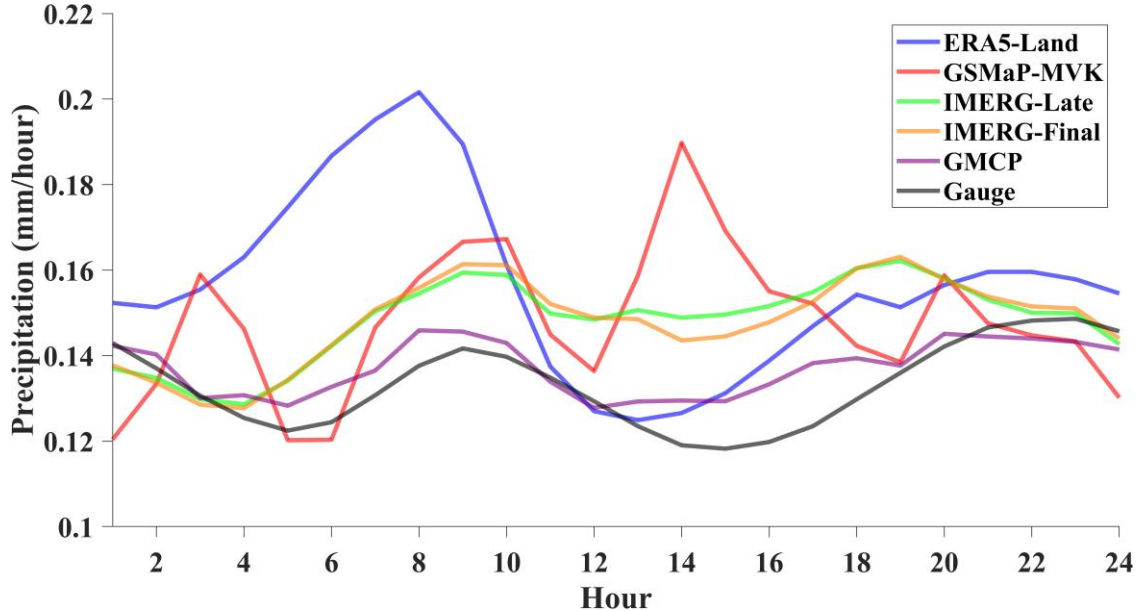


Figure 6. Average diurnal cycles based on ERA5-Land, GSMAp-MVK, IMERG-Late, IMERG-Final, GMCP and Gauges, at the corresponding $\sim 67,000$ rain gauges, in the period from January 1, to December 31, 2016, over Mainland China.

The ground gauge-based analysis APHRODITE_Japan Version 1207, which featured the highest resolution of 0.05° and operated on a daily scale for the period from January 1, 2009, to December 31, 2016 (Kamiguchi et al., 2010), was used as the ground truth to evaluate ERA5-Land, GSMAp-MVK, IMERG-Late, IMERG-Final, and GMCP on a daily scale, as shown in Figure 7. In terms of CC values, GMCP generally performed the best across Japan, with CC values exceeding 0.8 in most regions, followed by ERA5-Land, whereas GSMAp-MVK exhibited the poorest performance, with CC values below 0.7 in most regions, particularly in northern Japan. Notably, IMERG-Final presented significant improvements over IMERG-Late, likely because of its calibration schemes. The mean CC values for GMCP, ERA5-Land, IMERG-Final, IMERG-Late, and GSMAp-MVK were approximately 0.83, 0.81, 0.77, 0.69, and 0.67, respectively. Regarding the RMSE values, GMCP demonstrated the smallest errors, with the values bellow 8.0 mm/day, thereby outperforming ERA5-Land. IMERG-Late

performed slightly better than GSMAp-MVK; however, both lagged behind IMERG-Final. The mean RMSE values for GMCP, ERA5-Land, IMERG-Final, IMERG-Late, and GSMAp-MVK were approximately 7.88, 8.68, 9.13, 11.37, and 11.52 mm/day, respectively. In terms of precipitation occurrences, GMCP achieved the best overall performance with a mean HSS value of approximately 0.68, notably surpassing ERA5-Land, which had a mean HSS value of approximately 0.63. Despite being calibrated by gauge analysis, IMERG-Final demonstrated limited improvements, with an HSS value of approximately 0.52, which was comparable to that of IMERG-Late and GSMAp-MVK, both of which have HSS values of approximately 0.51.

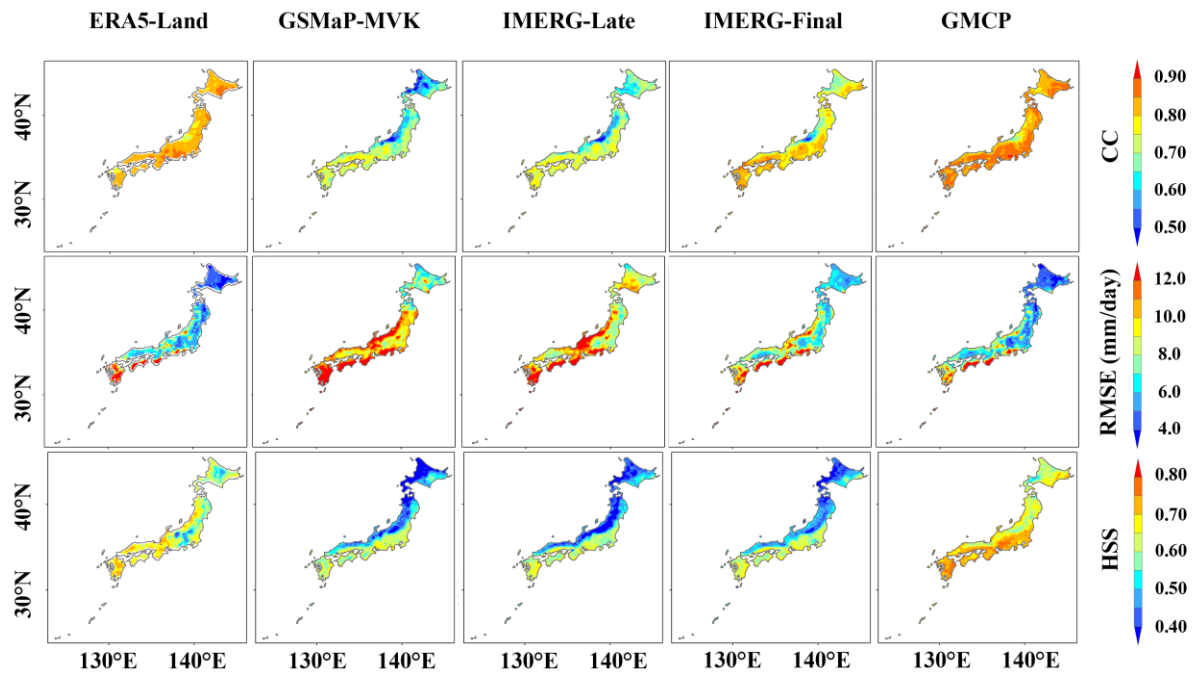


Figure 7. Spatial distributions of three verification metrics (CC, RMSE, and HSS) of precipitation datasets, ERA5-Land, GSMAp-MVK, IMERG-Late, IMERG-Final, and GMCP, against APHRODITE_Japan as the reference, at 0.05° and daily scales over Japan, in the entire period of APHRODITE_Japan from January 1, 2009, to December 31, 2016.

4.3 Case studies

To further investigate the performance of GMCP, ERA5-Land, GSMAp-MVK, IMERG-Late, and IMERG-Final against ground observations, we focused on the analysis of two regional extreme rainfall systems: Hurricane Zeta, which affected the southeastern CONUS, and Typhoon Haima, which affected Mainland China. A detailed examination of these events is provided below.

Hurricane Zeta. GMCP was validated during the landfall of Hurricane Zeta from 1600 UTC on October 28, 2020, to 1600 UTC on October 29, 2020, focusing on both spatial distributions and quantitative comparisons against the Stage IV gauge-radar (Figure 8). Overall, GMCP exhibited the most similar patterns to Stage IV in spatial distribution, followed by ERA5-Land (Figures 8a, 8e, and 8f), whereas the satellite-based products GSMAp-MVK, IMERG-Late, and IMERG-Final tended to overestimate the precipitation events in northeastern CONUS (Figures 8b, 8c, and 8d), with an overestimation of precipitation volumes approximately 20% (Figures 8h, 8i, and 8j). Additionally, GMCP demonstrated the superior performance against Stage IV, achieving the highest CC of 0.91, along with the smallest Bias of 0.76% and RMSE of 10.46 mm/hour, while ERA5-Land recorded the CC, Bias, and RMSE values of approximately 0.86, -4.56%, and 12.62 mm/hour, respectively. In contrast, all satellite-based products, including GSMAp-MVK, IMERG-Late, and IMERG-Final, exhibited significant errors with RMSE values of approximately 20.0 mm/hour, nearly double those of GMCP and ERA5-Land. A comparison of IMERG-Late and IMERG-Final revealed improvements only in CC and RMSE, whereas the Bias worsened, indicating the potential for further enhancements in the calibration strategies.

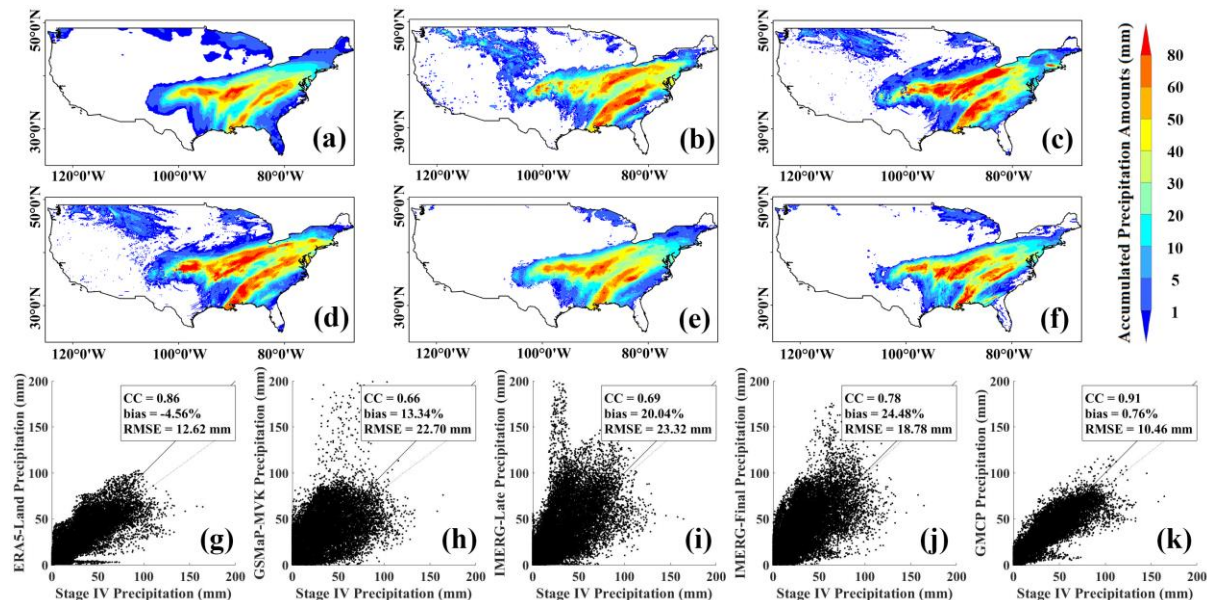


Figure 8. Spatial patterns of accumulated precipitation from (a) ERA5-Land, (b) GSMAp-MVK, (c) IMERG-Late, (d) IMERG-Final, (e) GMCP, and (f) Stage IV gauge-radar for Hurricane Zeta events from 1600 UTC October 28, 2020 to 1600 UTC October 29, 2020, and scatterplots of accumulated precipitation from (g) ERA5-Land, (h) GSMAp-MVK, (i) IMERG-Late, (j) IMERG-Final, and (k) GMCP against Stage IV gauge-radar for Hurricane Zeta events from 1600 UTC October 28, 2020 to 1600 UTC October 29, 2020.

Typhoon Haima. GMCP was evaluated during the landfall of Typhoon Haima over southeastern Mainland China from 0000 UTC on August 21, 2016 to 0000 UTC on August 22,

2016, focusing on both spatial distributions and quantitative comparisons against rain gauge-based interpolations (Figure 9). Overall, GMCP outperformed the other products with the highest CC of 0.54, along with the smallest Bias of 3.58% and RMSE of 3.04 mm/hour. In contrast, ERA5-Land tended to overestimate the precipitation volumes in its spatial distribution (Figure 9a) and exhibited a larger Bias of approximately 20% (Figure 9g), which was approximately five times greater than that of GMCP. Additionally, while model-based ERA5-Land generally performed worse than the satellite-based products GSMaP-MVK, IMERG-Late, and IMERG-Final in terms of Bias, it demonstrated better performances in terms of CC and RMSE.

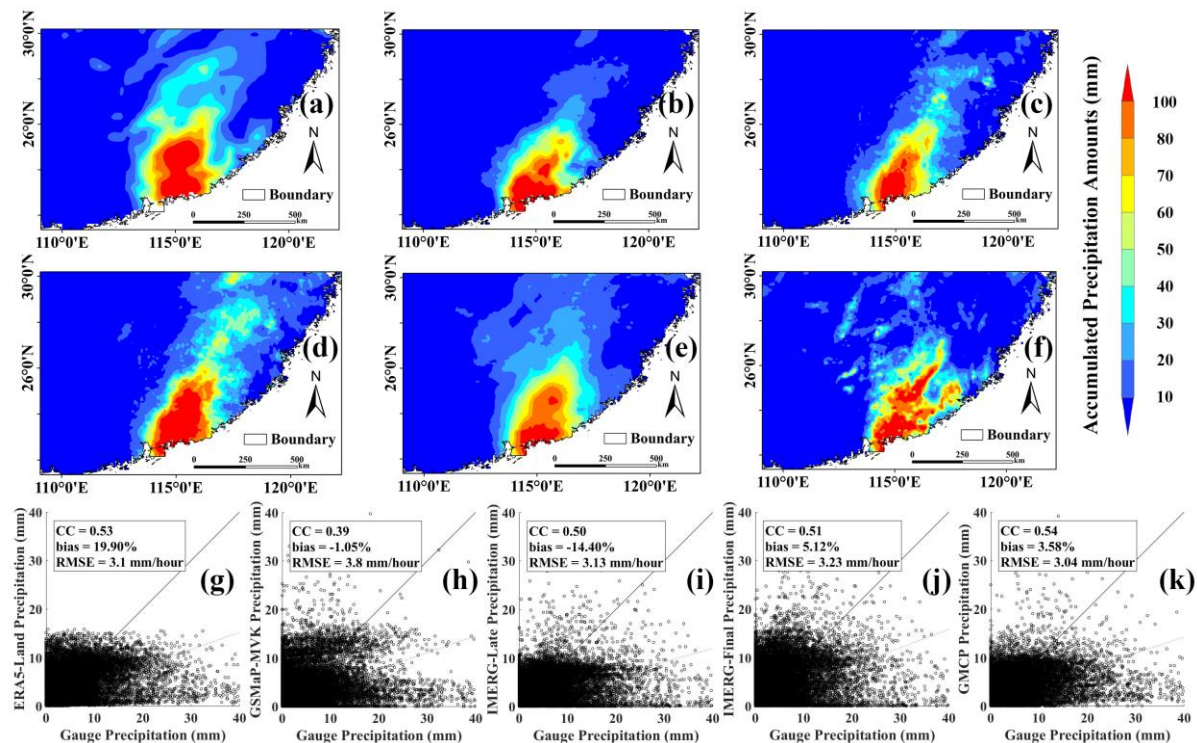


Figure 9. The spatial patterns of precipitation measured by (a) ERA5-Land, (b) GSMaP-MVK, (c) IMERG-Late, (d) IMERG-Final, (e) GMCP, and (f) rain gauge reference from 0000 UTC August 21, 2016 to 0000 August 22, 2016, and scatterplots of (g) ERA5-Land, (h) GSMaP-MVK, (i) IMERG-Late, (j) IMERG-Final, and (k) GMCP plotted against rain gauge observations during Typhoon Haima, which occurred from 0000 UTC August 21, 2016 to 0000 August 22, 2016.

5. Discussion

5.1 Comparisons between GMCP and MSWEP V2 at 3-hourly scale against rain gauges over Mainland China

MSWEP V2 (3-hourly, 0.1° , global, 1979–present) was the first fully global precipitation dataset derived primarily from the weighted average of precipitation volumes from nine datasets, including gauge, satellite, and reanalysis approaches, including daily gauge data, GPCC FDR, WorldClim, CMAP 1707, GPCC 2015, GPCP2.3, CMORPH, TMPA 3B42RT, Gridsat, CHIRPS 2.0, GSMAP, HOAPS3.2, JRA-55, ERA-Interim, and MERRA-2 (Beck et al., 2019). This dataset has been successfully applied at global and regional scales for various purposes such as water resource reanalysis and climatological and weather investigations (Beck et al., 2017). Hence, this study compared the performances of GMCP and MSWEP V2 at scales of 0.1° and 3-hourly against approximately 67, 000 rain gauges over Mainland China during the period from January 1, to December 31, 2016, as shown in Figure 10. Although GMCP performed slightly better than MSWEP V2 in terms of continuous verification diagnostics, with CC and RMSE values of approximately 0.52 and 1.94 mm/3-hourly, compared to 0.50 and 1.96 mm/3-hourly for MSWEP V2, it demonstrated the significant improvements in accurately capturing the precipitation occurrences. The HSS for GMCP was approximately 0.48, compared to 0.40 for MSWEP V2, indicating a notable improvement of approximately 20% in accurately detecting precipitation occurrences. Moreover, the analysis of spatial distribution reveals an anomalous region in northeastern Mainland China within the MSWEP V2 dataset (Figures 10a, 10c, and 10e), characterized by abnormally lower CC and HSS values and larger RMSE, which were not present in the GMCP dataset (Figure 10b, 10d, and 10f).

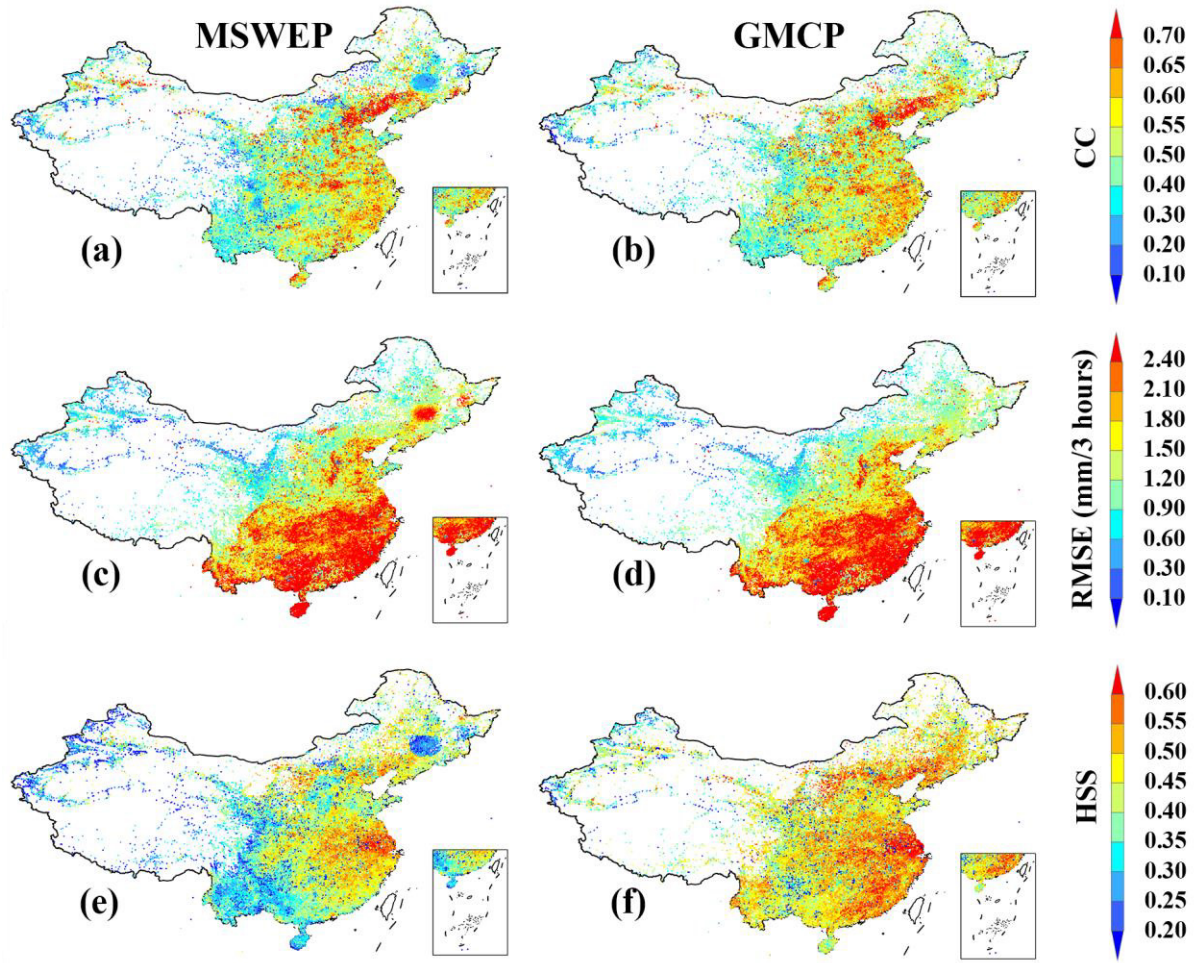


Figure 10. Spatial distributions of three verification metrics (CC, RMSE, and HSS) over Mainland China of GMCP and MSWEP V2 against ~ 67,000 rain gauges as the reference at scales of 3-hourly and 0.1° in the period from January 1, to December 31, 2016.

5.2 Comparisons between GMCP and CHIRPS at daily scale against rain gauges over Mainland China

CHIRPS is also a multi-source merged precipitation product (daily, 0.05° , 1981–present, 60°S – 60°N ; Funk et al., 2015), that incorporates five satellite products: Tropical Rainfall Measuring Mission 2B31 microwave precipitation estimates (Huffman et al., 2007), CMORPH microwave-plus-infrared-based precipitation estimates (Joyce et al., 2004), geostationary infrared brightness temperatures (Janowiak et al., 2001), and land surface temperature estimates (Wan et al., 2008). When missing TIR values resulted in absent precipitation estimates, these gaps were filled using CFS version 2 reanalysis fields (Saha et al., 2010). Additionally, CHIRPS utilizes various public gauge-based information and private archives, including GHCN monthly, GHCN daily, Global Summary of the Day (GSOD), GTS, and

additional observations from national meteorological agencies, primarily in Mexico, Central America, South America, and sub-Saharan Africa (Beck et al., 2013; Harris et al., 2014; Matsuura et al., 2009; Schneider et al., 2013; Funk et al., 2015).

Although CHIRPS integrated gauge-, satellite-, and model-based precipitation information, it performed notably worse than GMCP against approximately 67,000 rain gauges over Mainland China from January 1 to December 31, 2016, as shown in Figure 11. In terms of CC, GMCP significantly outperformed CHIRPS, with the mean CC values of approximately 0.74 and 0.47, respectively. GMCP also demonstrated the considerably smaller errors with mean RMSE values approximately 6.33 mm/day compared to approximately 10.24 mm/day for CHIRPS, particularly in southeastern China. Regarding the precipitation occurrences, GMCP achieved mean HSS values of approximately 0.58, greatly surpassing CHIRPS's mean HSS values of approximately 0.33 at almost all gauges. Overall, GMCP performed nearly twice as well as CHIRPS in terms of CC, RMSE, and HSS.

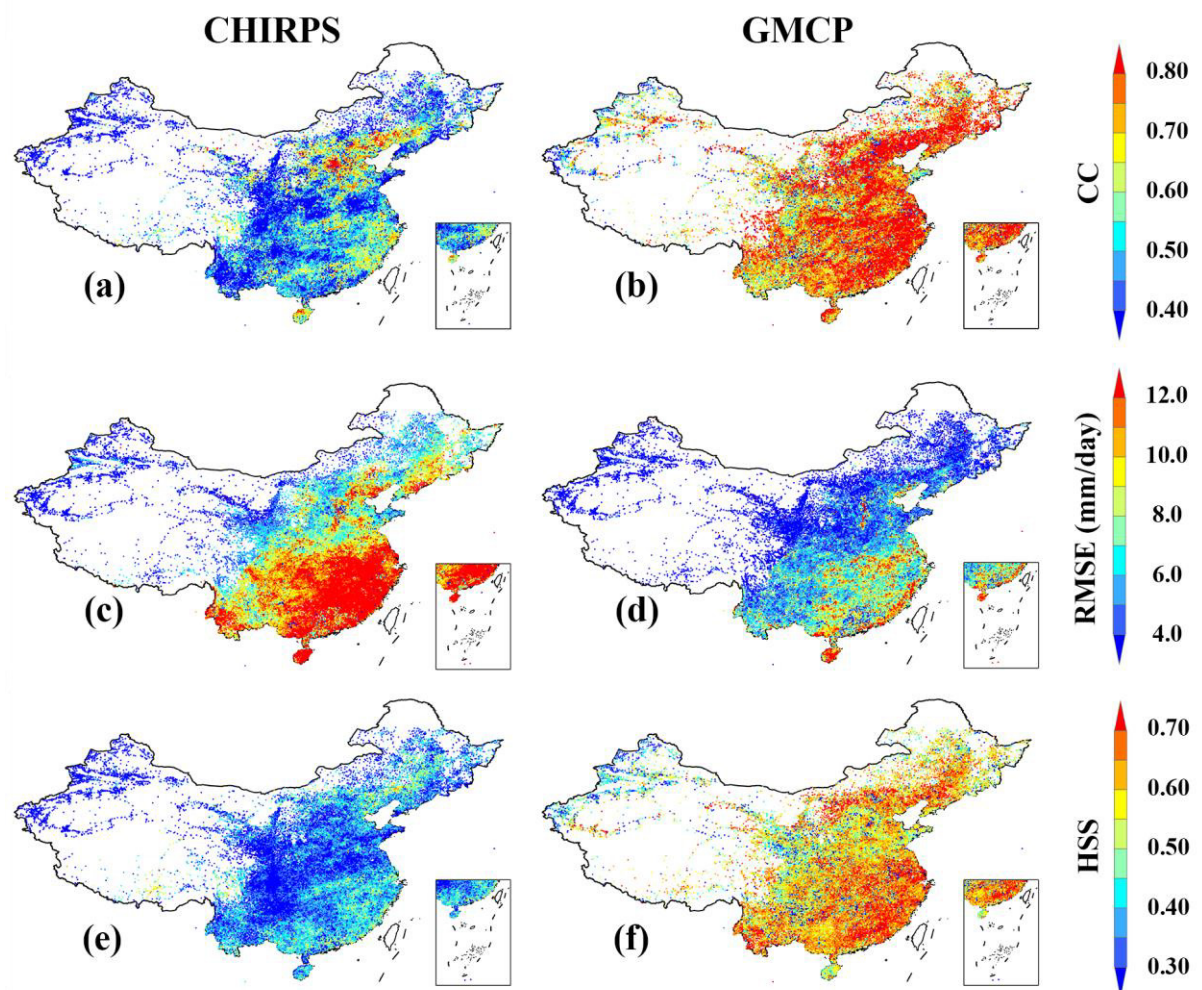


Figure 11. Spatial distributions of three verification metrics (CC, RMSE, and HSS) over Mainland China of GMCP and CHIRPS against ~ 67,000 rain gauges as the reference at scales of daily and 0.1° in the period from January 1 to December 31, 2016.

5.3 Potential reasons for the significant performance of the diagnostic indicators Considering the merging of precipitation occurrences

GMCP demonstrated robustness in merging multi-source precipitation products in terms of both volume and occurrence, particularly by significantly improving the accuracy of precipitation occurrence capture through the optimal integration of advantages and mitigation of the negative effects from various precipitation products. The robustness of GMCP was underpinned by at least three key factors: (1) the application of morphological theory to optimally identify the precipitation occurrence weights on a daily scale (Zhu et al., 2022); (2) a strategy that considers the hourly precipitation occurrences while merging their volumes based on the multiplicative triple collocation method (Stoffelen, 1998; Alemohammad et al., 2015; Lyu et al., 2021; Ji et al., 2024); and (3) calibration procedures applying the daily multi-source merging results to calibrate the hourly merged outcomes under total volume control strategy from AIMERG and AERA5-Asia (Ma et al., 2020, 2022). Specifically, GMCP identified precipitation occurrences according to the morphological characteristics of precipitation occurrence maps, a principle fundamentally distinct from methods such as MSWEP V1 and V2 (Beck et al., 2017, 2019), which could first directly remove precipitation occurrences with small precipitation volumes. In contrast, GMCP evaluated the reliability of precipitation occurrences based on their spatial features by applying morphological and optimal theories to assess the reliability of these features across each precipitation product. In the GMCP merging process, even pixels with large volumes from multi-source datasets may be excluded if deemed unreliable. GMCP can generally assign larger weights to pixels located closer to the center of the spatial continuous precipitation occurrence maps, as these pixels exhibited greater reliability and were more likely to be identified as precipitation occurrences owing to their larger morphological features. Conversely, smaller weights were assigned to the pixels farther away from the center, which were more likely to be classified as no-rain events. Ultimately, rain gauge-based observations were incorporated to finalize the final weight assignment in the merging process from the multi-source precipitation products (Zhu et al., 2022).

5.4 Potential future directions

Future improvements in GMCP can be pursued in at least two directions. First, dynamically optimizing the parameters in the GMCP model using regional gauge-based observations from dense and high-quality networks can enhance the reliability and accuracy of the dataset, particularly in mountainous and oceanic areas, at both daily and hourly scales. Second, merging additional gridded precipitation datasets from models and/or satellite-based retrievals may provide insights into the robustness of GMCP when simultaneously integrating a broader array of multi-source precipitation products.

The GMCP dataset spans the period from 2000 to the present and offers 1-hourly and 0.1° resolutions that remains open for global evaluations and applications. These efforts not only emphasized the dataset's current value but also revealed avenues for ongoing refinements, ensuring its utility in hydrological, climatological, and meteorological research, as well as in societal applications worldwide.

6. Data Availability

GMCP (1-hourly, 0.1° , global, 2000–2024) could be freely accessible at <https://doi.org/10.11888/Atmos.tpdc.301878> through the National Tibetan Plateau / Third Pole Environment Data Center.

7. Conclusions

There is an urgent need for fully global gridded precipitation estimates with long-term, high accuracy, and fine resolution for various scientific research and societal applications. The optimal merging of multi-source precipitation products has been explored extensively. To address the current limitations in considering precipitation occurrences, this study proposed a novel and flexible multi-source merging-and-calibration strategy that comprehensively integrated both precipitation volumes and occurrences, utilizing morphological theory, optimal theory, multiplicative triple collocation theory, and merging-and-calibration strategy, thereby generating a new fully global precipitation dataset, GMCP (1-hourly, 0.1° , global, 2000–Present). Initial evaluations yielded several key conclusions.

(1) The merging-and-calibration framework effectively integrated the advantages of gauge-, model-, and satellite-based precipitation estimates on a global scale while notably alleviating the negative effects associated with each input dataset.

(2) GMCP (1-hourly, 0.1°, global, 2000–Present) generally outperformed ERA5-Land, GSMAp-MVK, and IMERG-Late across various spatiotemporal scales, demonstrating the superior performance in regional statistics and extreme precipitation systems throughout almost the TRMM–GPM era.

(3) Despite IMERG-Final being calibrated with gauge analysis at the monthly scale, GMCP notably outperformed IMERG-Final, demonstrating the improvements in CC, RMSE, and HSS of approximately 66.67%, 39.25%, and 26.83%, respectively, during the period from January 1, 2016 to December 31, 2020, over CONUS against the gauge-radar-based Stage IV. This performance highlighted the significant potential of the merging-and-calibration framework for integrating the advantages of multi-source precipitation products at a resolution of 1-hourly and 0.1°.

(4) Compared with the state-of-the-art multi-source merged fully global precipitation dataset, MSWEP V2, GMCP outperformed MSWEP V2 in both precipitation volumes and occurrences, with notable improvements in accurately capturing precipitation occurrences, yielding HSS values of approximately 0.48 and 0.40, respectively, which indicated an improvement of approximately 20% against approximately 67, 000 rain gauges in 2016 over Mainland China at a resolution of 3-hourly and 0.1°.

(5) Compared with another well-known multi-source merged quasi-global daily and 0.05° precipitation product, CHIPRS, integrating the gauge-, satellite-, and reanalysis-based precipitation estimates, GMCP demonstrated notable improvements on a daily scale, achieving enhancements in CC, RMSE, and HSS by approximately 57.45%, 38.18%, and 75.76%, respectively, against approximately 67,000 rain gauges over Mainland China in 2016.

(6) The GMCP dataset could serve as a valuable gridded precipitation data for global scientific research and societal applications.

The results of this study indicate that the merging-and-calibration framework can serve as a valuable reference for multi-source merging schemes aimed at generating high-quality global precipitation products for both scientific research and operational purposes.

Acknowledgments.

This study is financially supported by the National Key R&D Program of China (Grant No. 2021YFB3900400); the Second Tibetan Plateau Scientific Expedition and Research (STEP)

program (grant no. 2019QZKK0105); the National Natural Science Foundation of China (Grant No. 42371335, 41901343); International Research Center of Big Data for Sustainable Development Goals Youth Director Foundation (CBAS2022DF011); the National Key R&D Program of China (Grant No. 2023YFB3905900); the China Postdoctoral Science Foundation (No. 2018M630037, and 2019T120021); the High-performance Computing Platform of Peking University; and also the National Tibetan Plateau / Third Pole Environment Data Center for continuously sharing the GMCP dataset. We also acknowledge use of the CPC-Gauge, ERA5, IMERG, GsMaP-MVK, GHCN and Stage IV data.

Data Availability Statement.

All the datasets used in this study are accessible.

REFERENCES

- Adler, R. F., and Coauthors, 2003: The version-2 global precipitation climatology project (GPCP) monthly precipitation analysis (1979–present). *J. Hydrometeorol.*, 4(6), 1147-1167, [https://doi.org/10.1175/1525-7541\(2003\)004<1147:TVGPCP>2.0.CO;2](https://doi.org/10.1175/1525-7541(2003)004<1147:TVGPCP>2.0.CO;2).
- Adler, R. F., and Coauthors, 2018: The Global Precipitation Climatology Project (GPCP) Monthly Analysis (New Version 2.3) and a Review of 2017 Global Precipitation. *Atmosphere*, 9, 138, <https://doi.org/10.3390/atmos9040138>.
- Alemohammad, S. H., and Coauthors, 2015: Characterization of precipitation product errors across the United States using multiplicative triple collocation. *Hydrol. Earth Syst. Sci.*, 19(8), 3489-3503, <https://doi.org/10.5194/hess-19-3489-2015>.
- Ashouri, H., and Coauthors, 2015: PERSIANN-CDR: Daily precipitation climate data record from multisatellite observations for hydrological and climate studies. *Bull. Amer. Meteorol. Soc.*, 96(1), 69-83, <https://doi.org/10.1175/BAMS-D-13-00068.1>.
- Baez-Villanueva, O. M., and Coauthors, 2020: RF-MEP: A novel Random Forest method for merging gridded precipitation products and ground-based measurements. *Remote Sens. Environ.*, 239, 111606, <https://doi.org/10.1016/j.rse.2019.111606>.
- Beck H.E., and Coauthors, 2017: MSWEP: 3-hourly 0.25° global gridded precipitation (1979–2015) by merging gauge, satellite, and reanalysis data. *Hydrol. Earth Syst. Sci.*, 21, pp. 589-615, <https://doi.org/10.5194/hess-21-589-2017>.

- Beck H.E., and Coauthors, 2019: MSWEP: V2 global 3-hourly 0.1 precipitation: methodology and quantitative assessment. *Bull. Am. Meteorol. Soc.*, 100(3), 473–500, <https://doi.org/10.1175/BAMS-D-17-0138.1>.
- Becker, A., and Coauthors, 2013: A description of the global land-surface precipitation data products of the Global Precipitation Climatology Centre with sample applications including centennial (trend) analysis from 1901-present. *Earth Syst. Sci. Data*, 5,71–99, <https://doi.org/10.5194/essd-5-71-2013>.
- Bhuiyan, M., Nikolopoulos, E. I., Anagnostou, E. N., P Quintana-Seguí, and Barella-Ortiz, A., 2018: A nonparametric statistical technique for combining global precipitation datasets: development and hydrological evaluation over the Iberian Peninsula, *Hydrol. Earth Syst. Sci.*, 22, 1371–1389, <https://doi.org/10.5194/hess-22-1371-2018>.
- Chen, M., and Xie, P., 2008: 3.3 Quality Control of Daily Precipitation Reports at NOAA/CPC, https://ftp.cpc.ncep.noaa.gov/precip.orig/CPC_UNI_PRCP/GAUGE_GLB/DOCU/CPC%20GTS%20QC%20AMS2008MingyueChen.pdf.
- Dee, D. P., and Coauthors, 2011: The ERA-Interim reanalysis: configuration and performance of the data assimilation system. *Q. J. R. Meteorol. Soc.*, 137(656), 553–597, <https://doi.org/10.1002/qj.828>.
- Douville, H., and Coauthors, 2021: Water cycle changes. In: Climate Change 2021: The Physical Science Basis. Contribution of Working Group I to the Sixth Assessment Report of the Intergovernmental Panel on Climate Change, V. Masson-Delmotte et al., Eds. (Cambridge Univ. Press, 2021), pp. 1055–1210, <https://doi.org/10.1017/9781009157896.010>.
- Du, J., 2011: NCEP/EMC 4KM Gridded Data (GRIB) Stage IV Data. Version 1.0. UCAR/NCAR - Earth Observing Laboratory. <https://doi.org/10.5065/D6PG1QDD>. Accessed 10 Aug 2022.
- Ebert, E. E., Janowiak, J. E., and Kidd, C., 2007: Comparison of near-real-time precipitation estimates from satellite observations and numerical models. *Bull. Am. Meteorol. Soc.*, 88(1), 47–64, <https://doi.org/10.1175/BAMS-88-1-47>.

- Funk, C., and Coauthors, 2015: The climate hazards infrared precipitation with stations—a new environmental record for monitoring extremes. *Sci. data*, 2(1), 1-21, <https://doi.org/10.1038/sdata.2015.66>.
- Gavahi, K., Foroumandi, E., and Moradkhani, H., 2023: A deep learning-based framework for multi-source precipitation fusion. *Remote Sens. Environ.*, 295, 113723, <https://doi.org/10.1016/j.rse.2023.113723>.
- Gelaro, R., and Coauthors, 2017: The modern-era retrospective analysis for research and applications, version 2 (MERRA-2). *J. Clim.*, 30(14), 5419-5454, <https://doi.org/10.1175/JCLI-D-16-0758.1>.
- Harris, I., Jones, P. D., Osborn, T. J. and Lister, D. H., 2014: Updated high-resolution grids of monthly climatic observations—the CRU TS3.10 Dataset. *Int. J. Climatol.*, 34, 623–642, <https://doi.org/10.1002/joc.3711>.
- Hersbach, H., and Coauthors, 2020: The ERA5 global reanalysis. *Q. J. R. Meteorol. Soc.*, 146(730), 1999-2049, <https://doi.org/10.1002/qj.3803>.
- Hou, A. Y., and Coauthors, 2014: The Global Precipitation Measurement Mission. *Bull. Amer. Meteorol. Soc.*, 95(5), 701-722, <https://doi.org/10.1175/BAMS-D-13-00164.1>.
- Hong, Y., Hsu, K.-L., Sorooshian, S., and Gao, X., 2004: Precipitation Estimation from Remotely Sensed Imagery Using an Artificial Neural Network Cloud Classification System, *J. Appl. Meteor.*, 43, 1834-1853, [10.1175/JAM2173.1](https://doi.org/10.1175/JAM2173.1).
- Huffman, G. J., and Coauthors, 1997: The global precipitation climatology project (GPCP) combined precipitation dataset. *Bull. Am. Meteorol. Soc.*, 78(1), 5-20, [https://doi.org/10.1175/1520-0477\(1997\)078%3C0005:TGPCPG%3E2.0.CO;2](https://doi.org/10.1175/1520-0477(1997)078%3C0005:TGPCPG%3E2.0.CO;2).
- Huffman, G. J., and Coauthors, 2007: The TRMM multisatellite precipitation analysis (TMPA): Quasi-global, multiyear, combined-sensor precipitation estimates at fine scales. *J. Hydrometeorol.*, 8(1), 38-55, <https://doi.org/10.1175/JHM560.1>.
- Huffman, G. J., Stocker, E.F., Bolvin, D.T., Nelkin, E.J., and Tan, J., 2019: GPM IMERG Final Precipitation L3 Half Hourly 0.1 degree x 0.1 degree V06, Greenbelt, MD, Goddard Earth Sciences Data and Information Services Center (GES DISC), <https://doi.org/10.5067/GPM/IMERG/3B-HH/06>.

- Huffman, G. J., and Coauthors, 2020: NASA Global Precipitation Measurement (GPM) Integrated Multi-satellitE Retrievals for GPM (IMERG), Algorithm Theoretical Basis Document (ATBD) Version 06., NASA/GSFC, Greenbelt, MD, USA, 39pp.
- Iguchi, T., and Meneghini, R. 2022: Stability of the Dual-Frequency Radar Equations and a New Method Applied to the GPM's Dual-Frequency Precipitation Radar (DPR) Data. *IEEE Trans. Geosci. Remote Sensing*, vol. 60, pp. 1-18, 2022, Art no. 5111818, doi: 10.1109/TGRS.2022.3159396.
- Ji, Q., Tang, G., Wu, S., Xu, J., Du, W., Peng, J., and Ma, Z., 2024: Multi-year evaluation of CloudSat, ERA5, and IMERG global snowfall products. *J. Hydrol.*, 131500, <https://doi.org/10.1016/j.jhydrol.2024.131500>.
- Jiang, J., and Coauthors, 2023: Precipitation regime changes in High Mountain Asia driven by cleaner air. *Nature*, 623(7987), 544-549, <https://doi.org/10.1038/s41586-023-06619-y>.
- Joyce, R. J., Janowiak, J. E., Arkin, P. A., and Xie, P., 2004: CMORPH: A Method that Produces Global Precipitation Estimates from Passive Microwave and Infrared Data at High Spatial and Temporal Resolution, *J. Hydrometeorol.*, 5, 487-503, 10.1175/1525-7541(2004)005<0487:CAMTPG>2.0.CO;2.
- Kidd, C., and Levizzani, V., 2011: Status of satellite precipitation retrievals. *Hydrol. Earth Syst. Sci.*, 15(4), 1109-1116, <https://doi.org/10.5194/hess-15-1109-2011>.
- Kobayashi, S., and Coauthors, 2015: The JRA-55 reanalysis: General specifications and basic characteristics. *J. Meteorol. Soc. Jpn. Ser. II*, 93(1), 5-48, <https://doi.org/10.2151/jmsj.2015-001>.
- Kubota, T., and Coauthors, 2007: Global Precipitation Map Using Satellite-Borne Microwave Radiometers by the GSMAp Project: Production and Validation. *IEEE Trans. Geosci. Remote Sensing*, 45(7), 2259-2275, <https://doi.org/10.1109/TGRS.2007.895337>.
- Kumar, A., Ramsankaran, R. A. A. J., Brocca, L., and Munoz-Arriola, F., 2019: A machine learning approach for improving near-real-time satellite-based rainfall estimates by integrating soil moisture. *Remote Sens.*, 11(19), 2221, <https://doi.org/10.3390/rs11192221>.
- Kummerow, C., Barnes, W., Kozu, T., Shiue, J., and Simpson, J., 1998: The Tropical Rainfall Measuring Mission (TRMM) Sensor Package, *J. Atmos. Ocean. Technol.*, 15, 809-817, 10.1175/1520-0426(1998)015<0809:TTRMMT>2.0.CO;2.

Kummerow, C. D., Randel, D. L., Kulie, M., Wang, N. Y., Ferraro, R., Joseph Munchak, S., and Petkovic, V., 2015: The evolution of the Goddard profiling algorithm to a fully parametric scheme. *J. Atmos. Ocean. Technol.*, 32(12), 2265-2280, <https://doi.org/10.1175/JTECH-D-15-0039.1>.

Lei, H., Zhao, H., and Ao, T., 2022: A two-step merging strategy for incorporating multi-source precipitation products and gauge observations using machine learning classification and regression over China. *Hydrol. Earth Syst. Sci.*, 26(11), 2969-2995, <https://doi.org/10.5194/hess-26-2969-2022>.

Levizzani, V., Kidd, C., Kirschbaum, D. B., Kummerow, C. D., Nakamura, K., and Turk, F. J., 2020: Satellite precipitation measurement. Cham, Switzerland: Springer, <https://doi.org/10.1007/978-3-030-24568-9>.

Lin, Y., and Mitchell, K. E., 2005: 1.2 the NCEP stage II/IV hourly precipitation analyses: Development and applications. In Proceedings of the 19th Conference Hydrology, American Meteorological Society, San Diego, CA, USA (Vol. 10).

Lu, H., Ding, L., Ma, Z., Li, H., Lu, T., Su, M., and Xu, J., 2020: Spatiotemporal Assessments on the Satellite - Based Precipitation Products From Fengyun and GPM Over the Yunnan - Kweichow Plateau, China. *Earth Space Sci.*, 7, e2019EA000857, <https://doi.org/10.1029/2019EA000857>.

Lyu, F., Tang, G., Behrangi, A., Wang, T., Tan, X., Ma, Z., and Xiong, W., 2020: Precipitation merging based on the triple collocation method across mainland China. *IEEE Trans. Geosci. Remote Sensing*, 59(4), 3161-3176, <https://doi.org/10.1109/TGRS.2020.3008033>.

Ma, Y., and Coauthors, 2018: Performance of optimally merged multisatellite precipitation products using the dynamic Bayesian model averaging scheme over the Tibetan Plateau. *J. Geophys. Res.-Atmos.*, 123(2), 814-834, <https://doi.org/10.1002/2017JD026648>.

Ma, Z., Shi, Z., Zhou, Y., Xu, J., Yu, W., and Yang, Y., 2017: A spatial data mining algorithm for downscaling TMPA 3B43 V7 data over the Qinghai - Tibet Plateau with the effects of systematic anomalies removed. *Remote Sens. Environ.*, 200, 378-395, <https://doi.org/10.1016/j.rse.2017.08.023>.

Ma, Z., He, K., Tan, X., Liu, Y., Lu, H., and Shi, Z., 2019: A new approach for obtaining precipitation estimates with a finer spatial resolution on a daily scale based on TMPA V7

- data over the Tibetan Plateau. *Int. J. Remote Sens.*, 40(22), 8465-8483, <https://doi.org/10.1080/01431161.2019.1612118>.
- Ma, Z., and Coauthors, 2020: An updated moving window algorithm for hourly-scale satellite precipitation downscaling: A case study in the Southeast Coast of China. *J. Hydrol.*, 581, 124378, <https://doi.org/10.1016/j.jhydrol.2019.124378>.
- Ma, Z., and Coauthors, 2020: AIMERG: a new Asian precipitation dataset (0.1° /half-hourly, 2000–2015) by calibrating the GPM-era IMERG at a daily scale using APHRODITE, *Earth Syst. Sci. Data*, 12, 1525-1544, <https://doi.org/10.5194/essd-12-1525-2020>.
- Ma, Z., and Coauthors, 2022: AERA5-Asia: A long-term Asian precipitation dataset (0.1° , 1 hourly, 1951–2015, Asia) anchoring the ERA5-Land under the total volume control by APHRODITE. *Bull. Am. Meteorol. Soc.*, 103(4), E1146-E1171, <https://doi.org/10.1175/BAMS-D-20-0328.1>.
- Ma, Z., Zhu, S., and Yang, J., 2022: FY4QPE-MSA: An all-day near-real-time quantitative precipitation estimation framework based on multispectral analysis from AGRI onboard Chinese FY-4 series satellites. *IEEE Trans. Geosci. Remote Sensing*, 60, 1-15, <https://doi.org/10.1109/TGRS.2022.3159036>.
- Manz, B., Buytaert, W., Zulkafli, Z., Lavado, W., Willems, B., Robles, L. A., and Rodríguez - Sánchez, J. P., 2016: High - resolution satellite - gauge merged precipitation climatologies of the Tropical Andes. *J. Geophys. Res.-Atmos.*, 121(3), 1190-1207, <https://doi.org/10.1002/2015JD023788>.
- Matsuura, K. and Willmott, C. J., 2009: Terrestrial precipitation: 1900–2008 gridded monthly time series. Center for Climatic Research Department of Geography Center for Climatic Research, University of Delaware. http://climate.geog.udel.edu/~climate/html_pages/Global_ts_2007/README.global.p_ts_2007.html.
- Mega, T., Ushio, T., Takahiro, M., Kubota, T., Kachi, M., and Oki, R., 2019, Gauge-Adjusted Global Satellite Mapping of Precipitation. *IEEE Trans. Geosci. Remote Sensing*, 57(4), 1928-1935, <https://doi.org/10.1109/TGRS.2018.2870199>.

- Meneghini, R., Liao, L., and Iguchi, T., 2022: A Generalized Dual-Frequency Ratio (DFR) Approach for Rain Retrievals, *J. Atmos. Ocean. Technol.*, 39(9), 1309-1329, <https://doi.org/10.1175/JTECH-D-22-0002.1>.
- Meng, H., and Coauthors, 2017: A 1DVAR - based snowfall rate retrieval algorithm for passive microwave radiometers. *J. Geophys. Res.-Atmos.*, 122(12), 6520-6540, <https://doi.org/10.1002/2016JD026325>.
- Muñoz-Sabater, J., 2019: First ERA5-Land dataset to be released this spring. ECMWF Newsletter, 159, 8-9, <https://www.ecmwf.int/en/newsletter/159/news/first-era5-land-dataset-be-released-spring>.
- NOAA National Centers of Environmental Information (NCEI), 1999: Global Surface Summary of the Day - GSOD. NOAA National Centers for Environmental Information. Accessed [2024-09-25].
- Sadeghi, M., Nguyen, P., Naeini, M. R., Hsu, K., Braithwaite, D., and Sorooshian, S. 2021: PERSIANN-CCS-CDR, a 3-hourly 0.04 global precipitation climate data record for heavy precipitation studies. *Sci. data*, 8(1), 157, <https://doi.org/10.1038/s41597-021-00940-9>.
- Saha, S., and Coauthors, 2010: The NCEP Climate Forecast System Reanalysis. *Bull. Amer. Meteor. Soc.*, 91, 1015–1057, <https://doi.org/10.1175/2010BAMS3001.1>.
- Schneider, U., and Coauthors, 2013: GPCC's new land surface precipitation climatology based on quality-controlled in situ data and its role in quantifying the global water cycle. *Theor. Appl. Climatol.*, 115, 15–40, <https://doi.org/10.1007/s00704-013-0860-x>.
- Shen, Y., Zhao, P., Pan, Y., and Yu, J., 2014: A high spatiotemporal gauge-satellite merged precipitation analysis over China, *J. Geophys. Res. Atmos.*, 119, <https://doi.org/10.1002/2013JD020686>.
- Sorooshian, S., Hsu, K. L., Gao, X., Gupta, H. V., Imam, B., and Braithwaite, D., 2000: Evaluation of PERSIANN system satellite-based estimates of tropical rainfall. *Bull. Am. Meteorol. Soc.*, 81(9), 2035-2046, [https://doi.org/10.1175/1520-0477\(2000\)081%3C2035:EOPSS%3E2.3.CO;2](https://doi.org/10.1175/1520-0477(2000)081%3C2035:EOPSS%3E2.3.CO;2).
- Stoffelen, A., 1998: Toward the true near - surface wind speed: Error modeling and calibration using triple collocation. *J. Geophys. Res.-Oceans*, 103(C4), 7755-7766, <https://doi.org/10.1029/97JC03180>.

- Tang, G., Clark, M. P., Papalexiou, S. M., Ma, Z., and Hong, Y., 2020: Have satellite precipitation products improved over last two decades? A comprehensive comparison of GPM IMERG with nine satellite and reanalysis datasets. *Remote Sens. Environ.*, 240, 111697, <https://doi.org/10.1016/j.rse.2020.111697>.
- Tang, Y., Yu, F., Pedrycz, W., Yang, X., Wang, J., and Liu, S., 2021: Building trend fuzzy granulation-based LSTM recurrent neural network for long-term time-series forecasting. *IEEE Trans. Fuzzy Syst.*, 30(6), 1599–1613, <https://doi.org/10.1109/TFUZZ.2021.3062723>.
- Tao, Y., Gao, X., Hsu, K., Sorooshian, S., and Ihler, A., 2016: A deep neural network modeling framework to reduce bias in satellite precipitation products. *J. Hydrometeorol.*, 17(3), 931–945, <https://doi.org/10.1175/JHM-D-15-0075.1>.
- Trenberth, K. E., Cheng, L., Jacobs, P., Zhang, Y., and Fasullo, J., 2018: Hurricane Harvey links to ocean heat content and climate change adaptation. *Earth Future*, 6(5), 730–744, <https://doi.org/10.1029/2018EF000825>.
- Wan, Z., 2008: New refinements and validation of the MODIS Land-Surface Temperature/Emissivity products. *Remote Sens. Environ.*, 112, 59–74, <https://doi.org/10.1016/j.rse.2006.06.026>.
- Wu, D., Hu, Z., Li, J., and Sun, X., 2021: Forecasting nonadiabatic dynamics using hybrid convolutional neural network/long short-term memory network. *J. Chem. Phys.*, 155(22), <https://doi.org/10.1063/5.0073689>.
- Xie, P., Chen, M., Yang, S., Yatagai, A., Hayasaka, T., Fukushima, Y., and Liu, C., 2007: A gauge-based analysis of daily precipitation over East Asia. *J. Hydrometeorol.*, 8(3), 607–626, <https://doi.org/10.1175/JHM583.1>.
- Xie, P., and Xiong, A. Y., 2011: A conceptual model for constructing high - resolution gauge - satellite merged precipitation analyses. *J. Geophys. Res.-Atmos.*, 116(D21), <https://doi.org/10.1029/2011JD016118>.
- Xu, J., Ma, Z., Tang, G., Ji, Q., Min, X., Wan, W., and Shi, Z., 2019: Quantitative Evaluations and Error Source Analysis of Fengyun-2-Based and GPM-Based Precipitation Products over Mainland China in Summer, 2018, *Remote Sens.*, 11(24), 2992, <https://doi.org/10.3390/rs11242992>.

- Xu, J., Ma, Z., Yan, S., and Peng, J., 2022: Do ERA5 and ERA5-land precipitation estimates outperform satellite-based precipitation products? A comprehensive comparison between state-of-the-art model-based and satellite-based precipitation products over mainland China. *J. Hydrol.*, 605, 127353, <https://doi.org/10.1016/j.jhydrol.2021.127353>.
- Xu, J., Ma, Z., Hu, H., and Weng, F., 2023: A cloud-dependent 1DVAR precipitation retrieval algorithm for FengYun-3D microwave soundings: a case study in tropical cyclone mekkhala. *IEEE Geosci. Remote Sens. Lett.*, 20, 1-5, <https://doi.org/10.1109/LGRS.2023.3243934>.
- Yan, S., Ma, Z., Li, X., Hu, H., Xu, J., Ji, Q., and Weng, F., 2023: PCSSR - DNNWA: A physical constraints based surface snowfall rate retrieval algorithm using deep neural networks with attention module. *Geophys. Res. Lett.*, 50(13), e2023GL103923, <https://doi.org/10.1029/2023GL103923>.
- Yatagai, A., Kamiguchi, K., Arakawa, O., Hamada, A., Yasutomi, N., and Kitoh, A., 2012: APHRODITE: Constructing a Long-Term Daily Gridded Precipitation Dataset for Asia Based on a Dense Network of Rain Gauges, *Bull. Amer. Meteor. Soc.*, 93, 1401-1415, <https://doi.org/10.1175/BAMS-D-11-00122.1>.
- Yatagai, A., Maeda, M., Masuda, M., Suetou, N., Yasutomi, N., and Khadgarai, S., 2019: Asian Precipitation—Highly-Resolved Observational Data Integration Towards Evaluation of Extreme Events (APHRODITE-2). IPSJ Tohoku Branch SIG Technical Report. 2018-9-A2-2. Available online: <http://www.topic.ad.jp/ipsj-tohoku/lib/exe/fetch.php?media=report:20180221-a2-2.pdf>.
- Yumnam, K., Guntu, R. K., Rathinasamy, M., and Agarwal, A., 2022: Quantile-based Bayesian Model Averaging approach towards merging of precipitation products. *J. Hydrol.*, 604, 127206, <https://doi.org/10.1016/j.jhydrol.2021.127206>.
- Zhang, W., and Coauthors, 2021: Increasing precipitation variability on daily-to-multiyear time scales in a warmer world. *Sci. Adv.*, 7(31), eabf8021, <https://doi.org/10.1126/sciadv.abf8021>.
- Zhang, W., Zhou, T., and Wu, P., 2024: Anthropogenic amplification of precipitation variability over the past century. *Science*, 385(6707), 427-432, <https://doi.org/10.1126/science.adp0212>.
- Zhang, Y., and Coauthors, 2023: Southern Hemisphere dominates recent decline in global water availability. *Science*, 382(6670), 579-584, <https://doi.org/10.1126/science.adh0716>.

Zhu, S., and Ma, Z., 2022: PECA-FY4A: Precipitation Estimation using Chromatographic Analysis methodology for full-disc multispectral observations from FengYun-4A/AGRI. *Remote Sens. Environ.*, 282, 113234, <https://doi.org/10.1016/j.rse.2022.113234>.

Zhu, S., and Coauthors, 2022: A morphology-based adaptively spatio-temporal merging algorithm for optimally combining multisource gridded precipitation products with various resolutions. *IEEE Trans. Geosci. Remote Sensing*, 60, 1-21, <https://doi.org/10.1109/TGRS.2021.3097336>.